

## ORIGINAL ARTICLE

# Modeling effects of dexamethasone on disease progression of bone mineral density in collagen-induced arthritic rats

Hoi-Kei Lon<sup>1</sup>, Debra C. DuBois<sup>2</sup>, Justin C. Earp<sup>3</sup>, Richard R. Almon<sup>2</sup> & William J. Jusko<sup>1</sup><sup>1</sup>Department of Pharmaceutical Sciences, School of Pharmacy and Pharmaceutical Sciences, University at Buffalo, Buffalo, New York 14214<sup>2</sup>Department of Biological Sciences, University at Buffalo, Buffalo, New York 14260<sup>3</sup>Center for Drug Evaluation and Research, U.S. Food and Drug Administration, Silver Spring, Maryland 20993**Keywords**

Biomarkers, bone modeling, dexamethasone, pharmacodynamics, systems model

**Correspondence**

William J. Jusko, 404 Kapoor Hall, Department of Pharmaceutical Sciences, University at Buffalo, State University of New York. Buffalo, NY 14214. Tel: 716-645-2855; Fax: 716-829-6569; E-mail: wjjusko@buffalo.edu

**Funding Information**

This work was supported by funding from the National Institutes of Health Grant GM 24211 and a fellowship for Lon from Amgen, Inc.

Received: 17 June 2015; Accepted: 23 June 2015

**Pharma Res Per**, 3(5), 2015, e00169, doi: 10.1002/prp2.169

doi: 10.1002/prp2.169

**Abstract**

A mechanism-based model was developed to characterize the crosstalk between proinflammatory cytokines, bone remodeling biomarkers, and bone mineral density (BMD) in collagen-induced arthritic (CIA) rats. Male Lewis rats were divided into five groups: healthy control, CIA control, CIA receiving single 0.225 mg kg<sup>-1</sup> subcutaneous (SC) dexamethasone (DEX), CIA receiving single 2.25 mg kg<sup>-1</sup> SC DEX, and CIA receiving chronic 0.225 mg kg<sup>-1</sup> SC DEX. The CIA rats underwent collagen induction at day 0 and DEX was injected at day 21 post-induction. Disease activity was monitored throughout the study and rats were sacrificed at different time points for blood and paw collection. Protein concentrations of interleukin (IL)-1 $\beta$ , IL-6, receptor activator of nuclear factor kappa-B ligand (RANKL), osteoprotegerin (OPG), and tartrate-resistant acid phosphatase 5b (TRACP-5b) in paws were measured by enzyme-linked immunosorbent assays (ELISA). Disease progression and DEX pharmacodynamic profiles of IL-1 $\beta$ , IL-6, RANKL, and OPG were fitted simultaneously and parameters were sequentially applied to fit the TRACP-5b and BMD data. The model was built according to the mechanisms reported in the literature and modeling was performed using ADAPT 5 software with naïve pooling. Time profiles of IL-1 $\beta$  and IL-6 protein concentrations correlated with their mRNAs. The RANKL and OPG profiles matched previous findings in CIA rats. DEX inhibited the expressions of IL-1 $\beta$ , IL-6, and RANKL, but did not alter OPG. TRACP-5b was also inhibited by DEX. Model predictions suggested that anti-IL-1 $\beta$  therapy and anti-RANKL therapy would result in similar efficacy for prevention of bone loss among the cytokine antagonists.

**Abbreviations**

(IL)-1 $\beta$ , interleukin-one-beta; AOB, active osteoblasts; AOC, active osteoclasts; AUEC, area under the effect curves; BCA, bichoninic acid; BMD, bone mineral density; CIA, collagen-induced arthritic; COX, cyclooxygenase; CST, corticosterone; DEX, dexamethasone; DF, diaphyseal femur; EDTA, ethylenediaminetetraacetic acid; EF, epiphyseal femur; ELISA, enzyme-linked immunosorbent assays; GR, glucocorticoid receptor; IL-6, interleukin-six; LR, lumbar vertebrae; M-CSF, macrophage-colony-stimulating factor; MF, metaphyseal femur; MMPs, metalloproteinases; mRNA, messenger ribonucleic acid; OPG, osteoprotegerin; PD, pharmacodynamic; PGE<sub>2</sub>, prostaglandin E<sub>2</sub>; PK, pharmacokinetic; PTH, parathyroid hormone; QC, quality control; RANKL, receptor activator of nuclear factor kappa-B ligand; RANK, receptor activator of nuclear factor kappa-B; RA, rheumatoid arthritis; ROB, responding osteoblasts; SC, subcutaneous; TGF- $\beta$ , transforming growth factor- $\beta$ ; TF, total femur; TNF- $\alpha$ , tumor necrosis factor- $\alpha$ ; TRACP-5b, tartrate-resistant acid phosphatase 5b.

## Introduction

Bone remodeling is a tightly controlled dynamic process that is regulated by many different factors. Two major cell types that are responsible for bone homeostasis are osteoblasts and osteoclasts. Osteoblasts are bone-forming cells that synthesize the bone matrix and mineralization. Osteoclasts are responsible for bone resorption (Tanaka *et al.* 2005). When the activity of osteoblasts exceeds that of osteoclasts, bone formation dominates as is the case during the growth period in childhood. In bone-related disease conditions such as osteoporosis and rheumatoid arthritis (RA), the activity of osteoclasts becomes dominant; active bone resorption occurs and leads to bone destruction. To understand the pathogenesis of bone loss in RA, it is important to study the mediators and pathways controlling the activities of osteoblasts and osteoclasts.

One of the major mechanisms governing the balance between osteoblasts and osteoclasts is the RANK/RANKL/OPG system. RANK (~67 kDa) is expressed on osteoclast precursors, and its activation is required for maturation of osteoclast precursors to active osteoclasts. This activation is mediated by the binding between RANK and RANKL (~35 kDa), which is a member of the tumor necrosis factor (TNF)-family of cytokines and is produced by osteoblasts. Upon maturation of osteoclasts, they can elicit their bone-resorbing activity and initiate the bone breakdown process. This process is counter-regulated by the action of OPG (~120 kDa as a homodimer), which is a natural decoy receptor for RANKL synthesized primarily by osteoblasts (Nelson *et al.* 2012). In healthy conditions, this system is at steady-state and is responsible for maintaining normal bone metabolism. However, in bone-related diseases, especially in immune diseases such as RA, the components in this system are under the influence of other immune stimulants, resulting in the disruption of the osteoblast/osteoclast balance.

Rheumatoid arthritis is characterized as a chronic inflammatory condition that is mediated mainly by immune cells such as macrophages and fibroblasts, as well as proinflammatory cytokines TNF- $\alpha$ , IL-1 $\beta$ , and IL-6 (Choy and Panayi 2001). The immune cascade caused by cytokines results in two parallel processes: joint inflammation and joint destruction. Joint inflammation is primarily driven by the cytokines and leads to pain and swelling. Joint destruction is partly driven by the inflammation process and has a more complicated pathology. It involves the effects of cytokines, the RANK/RANKL/OPG system, together with other factors such as metalloproteinases (MMPs) (Klareskog *et al.* 2009). Our laboratory

previously published a mechanism-based model that described the dynamics and the interplay between DEX, endogenous corticosterone (CST), glucocorticoid receptor (GR), proinflammatory cytokines (TNF- $\alpha$ , IL-1 $\beta$ , and IL-6), and their regulation of disease endpoints (paw swelling and bone mineral density) in rats with collagen-induced arthritis, which is a common animal model of RA (Earp *et al.* 2008a,b). The current study aimed to further expand this model with added information regarding the temporal changes of the components in the RANK/RANKL/OPG pathway and osteoclast activity, and thus provide better insights into bone destruction in RA.

Many mathematical models were published exploring the dynamics of bone remodeling with the incorporation of the RANK/RANKL/OPG signaling pathway (Pivonka *et al.* 2008, 2010; Peterson and Riggs 2010, 2012; Schmidt *et al.* 2011; Post *et al.* 2013). Most were built according to literature findings and focused on the effects of calcium and hormones such as parathyroid hormone (PTH) and transforming growth factor (TGF)- $\beta$  on bone remodeling. They adequately predict BMD progression under different situations such as aging, osteoporosis, and sustained glucocorticoid therapy, and are also useful in making recommendations for therapeutic interventions that may lead to desirable clinical outcomes. However, to our knowledge, no such model has been developed for RA. Our current study develops a similar mechanism-based model for RA and includes experimental data regarding RANKL and OPG disease progression. The model presented in this study is a combination of our Earp *et al.* model developed for CIA disease progression and the bone remodeling model developed by Lemaire *et al.* (2004). The model as a whole characterizes the crosstalk between the immune cascade, the RANK/RANKL/OPG pathway, as well as BMD during RA disease progression.

## Materials and Methods

### Animals

Male Lewis rats (6–9 weeks old) were purchased from Harlan (Indianapolis, IN) with weights of 150–175 g. The rats were housed individually in the University Laboratory Animal Facility and acclimatized for 1 week under constant temperature (22°C), humidity (72%), and 12-h light/12-h dark cycle. Rats had free access to rat chow and water. All protocols followed the Principles of Laboratory Animal Care (Institute of Laboratory Animal Resources, 1996) and were approved by the University at Buffalo Institutional Animal Care and Use Committee.

## Induction of collagen-induced arthritis in Lewis rats

The induction of collagen-induced arthritis (CIA) in Lewis rats followed protocols and reagents supplied by Chondrex, Inc. (Redmond, WA). The day of first collagen induction was regarded as day 0 in the study. Detailed procedures of the collagen induction were described previously (Earp et al. 2008b; Lon et al. 2011).

## Experimental design

A number of rats were assigned as healthy controls and did not undergo collagen induction. One or two healthy control rats were sacrificed on days 9, 15, 19, 21, 23, 30, and 34 for baseline assessment. For CIA rats, paw edema and body weights were monitored throughout the entire study starting from day 0. Paw sizes were determined using digital calipers with details described previously (Earp et al. 2008a,b, 2009; Liu et al. 2011; Lon et al. 2011). Edema was indicated by the sum of the paw and ankle area measurements for each hind foot. On day 20 post-induction, rats with paw volume increases of at least 50% in one or two paws were selected and randomly assigned to four groups: vehicle control group, SC low-dose group which received 0.225 mg kg<sup>-1</sup> subcutaneous (SC) DEX on day 21, SC high-dose group which received 2.25 mg kg<sup>-1</sup> SC DEX on day 21, and SC multiple-dose group which received once a day doses of 0.225 mg kg<sup>-1</sup> SC DEX on days 21–27. For the CIA control group, one to four rats were sacrificed on days 9, 15, 19, 21, 23, 30, 34, and 40. For the DEX groups, three or four rats were sacrificed at each time point. For rats in the SC low-dose and high-dose groups, these time points were at 1, 2, 4, 6, 8, 12, 24, 36, 48, 96, 216, and 336 h after dosing, while for SC multiple-dose rats, time points were at 36, 84, 132, 180, 264, and 336 h after the first dose.

All rats were sacrificed by aortal exsanguinations and blood was collected in syringes containing EDTA as anti-coagulant. Blood samples were centrifuged at 2000g for 10 min at 4°C. Plasma was then collected and aliquots were transferred into microfuge tubes. Paw tissues (above ankle excluding skin and toenails) were also collected during the sacrifice and were flash-frozen in liquid nitrogen. After collection, all blood and paw samples were immediately stored at –80°C before further analysis.

## Protein extraction from the rat paws

Frozen paw tissue was pulverized with a mortar and pestle under liquid nitrogen. For CIA rats, only swollen paws (indicated by paw edema measurements) were processed and included in our analysis. The protein extraction

buffer was composed of 50 mmol L<sup>-1</sup> Tris buffer at pH 7.4, 0.1 mol L<sup>-1</sup> NaCl, and 0.1% Triton X-100 with the addition of protease inhibitor cocktail from Roche (cOmplete, Mini; one tablet per 10 mL buffer, Indianapolis, IN). The composition of the buffer was reported previously for protein extraction (Stolina et al. 2008, 2009). Pulverized paw tissue was weighed in a polypropylene tube and mixed with the protein extraction buffer. The mixture was then homogenized using a Kinematica Polytron homogenizer (model PT10-35; Kinematica Inc., Newark, NJ) on speed setting at five in an ice-bath for three 10-sec durations, with a 30-sec interval for cooling. The homogenization probe was rinsed three times with double distilled water, chilled with ice, and completely dried between samples. The homogenate was transferred to a centrifuge tube and centrifuged at 10,000 rpm for 10 min. The supernatant was collected and aliquots were stored at –80°C. Total protein concentrations in the homogenate samples were determined using the microplate procedure with a BCA assay kit (Pierce Biotechnology, Rochford, IL).

## Measurements of protein concentration by ELISA methodology

Concentrations of IL-1 $\beta$ , IL-6, RANKL, OPG, and TRACP-5b in paw homogenates were determined by ELISA. For IL-1 $\beta$ , IL-6, and RANKL, undiluted homogenates were added during the ELISA procedure. For TRACP-5b, homogenates were diluted two- to four-fold with homogenization buffer before analysis. The assay results were normalized with the total protein concentrations obtained by the BCA assay. For OPG, protein concentrations of the homogenate samples were adjusted to 1 mg mL<sup>-1</sup> before the procedure to minimize the matrix effects observed in a preliminary test.

Quantikine Rat Immunoassay kits from R&D Systems, Inc. (Minneapolis, MN) were used for measuring concentrations of IL-1 $\beta$  and IL-6. Quantikine Mouse RANKL Immunoassay kit from the same company was used for rat RANKL protein determination. This use is based on the high (96%) similarity between the mouse and rat RANKL amino acid sequence (Xu et al. 2000) and its successful application reported previously (Stolina et al. 2005). Osteoprotegerin ELISA kit (for mouse/rat OPG) from Alpco Diagnostics (Salem, NH) was used for measuring OPG. RatTRAP assay kit from Immunodiagnostic Systems Ltd (IDS Ltd, Fountain Hills, AZ) was used for TRACP-5b. The assay procedures followed the manufacturers' instructions. All samples were run in duplicate and quality control (QC) samples were prepared for each plate for between-assay variability assessment. Calibration curves for IL-1 $\beta$ , IL-6, and RANKL were constructed by

plotting the absorbance of each standard versus its concentration on a log/log graph with the best-fitted line determined by regression analysis. Calibration curves for OPG and TRACP-5b were built by fitting the standards and the absorbance readings into a 4-parameter logistic model. The lower limits of quantification for IL-1 $\beta$ , IL-6, RANKL, OPG, and TRACP-5b were 31.2, 62.5, 31.2, 62.5 pg mL<sup>-1</sup>, and 0.52 U L<sup>-1</sup>. The between-assay coefficients of variability were 7.86%, 9.09%, 3.35%, 8.49%, and 2.01%.

**Mechanism-based disease progression model**

Figure 1 displays a schematic of the mechanistic model. The components describing the dynamics of corticosteroids

terone (CST), glucocorticoid receptor (GR) mRNA, and the three proinflammatory cytokines (TNF- $\alpha$ , IL-1 $\beta$ , and IL-6) mRNAs utilized our previous model (Earp et al. 2008a,b). Intramuscular (IM) DEX PK characteristics in both healthy and CIA rats have been investigated (Earp et al. 2008c), and preliminary study has shown the similarity between IM and SC PK profiles. Thus, the IM PK model was used for SC DEX. All parameters regarding these components were fixed in the analysis, except for  $\alpha_2$  (0.0002894 nmol GR nmol IL-1 $\beta$ <sup>-1</sup>) and  $\beta_2$  (0.00001159 ng CST mL<sup>-1</sup> GR nmol IL-1 $\beta$ <sup>-1</sup>), which describe the intrinsic activity of IL-1 $\beta$  on GR mRNA and CST as described in the Earp et al. article. These two values are close to zero and simulations indicated that their removal did not alter the model fittings; thus these two parameters were fixed to 0 for simplicity. The time

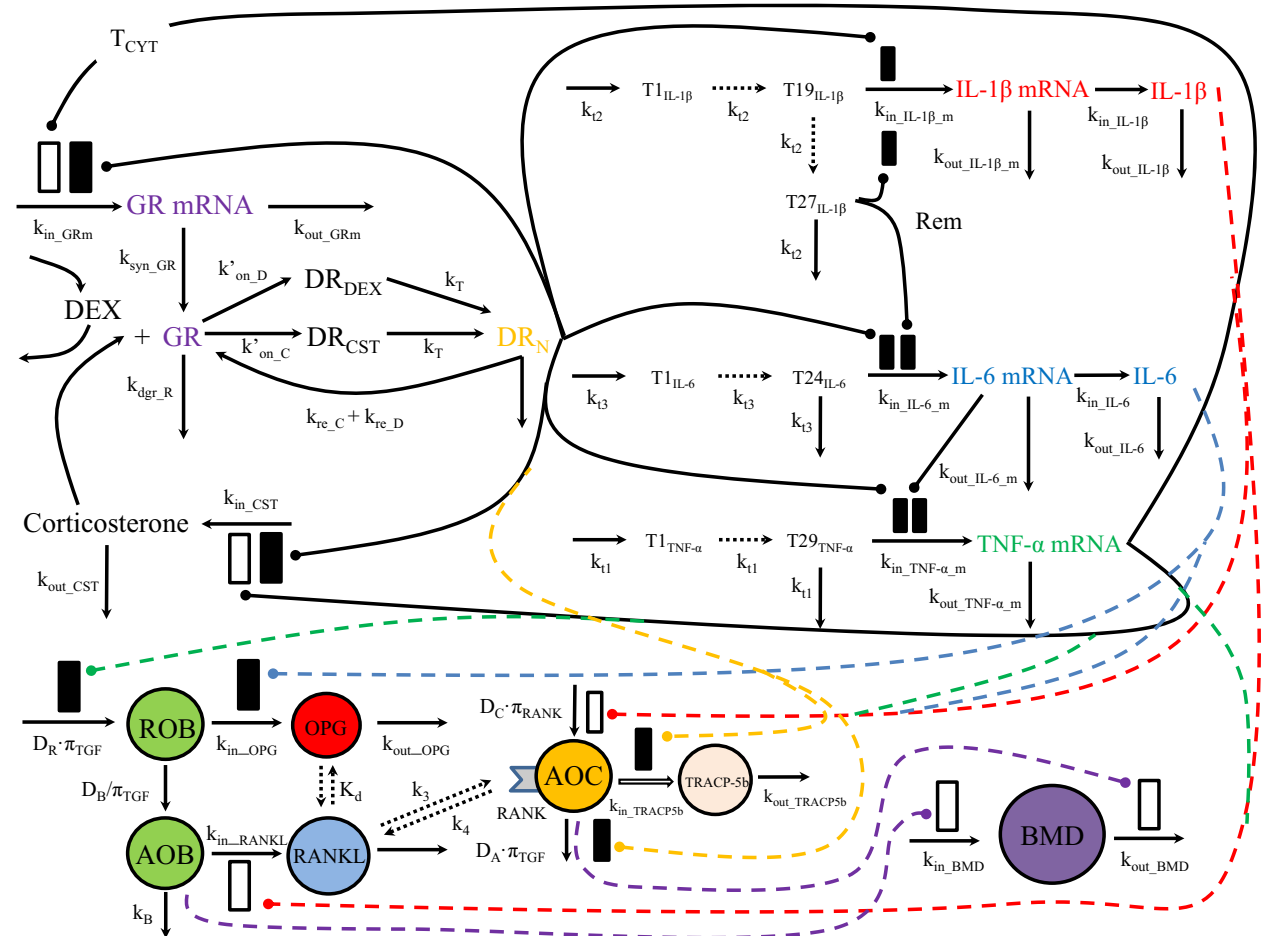


**Figure 1.** Schematic of the mechanistic model of disease progression of glucocorticoid receptor (GR), proinflammatory cytokines (TNF- $\alpha$ , IL-1 $\beta$ , and IL-6), RANK/RANKL/OPG system, and bone mineral density (BMD) in collagen-induced arthritic (CIA) rat model. The bone homeostasis-related components of the model are displayed in colored circles. Black solid lines indicate the interactions described by the previous Earp model. Dashed lines specify the action of IL-1 $\beta$  (red), IL-6 (blue), and TNF- $\alpha$  (green) on different components of the bone remodeling system. Yellow-dashed lines indicate the action of DR<sub>N</sub> on active osteoclasts (AOC) and its activity, and purple dashed lines show the action of active osteoblasts (AOB) and AOC on BMD. CIA, collagen-induced arthritic; RANKL, receptor activator of nuclear factor kappa-B ligand.

profiles of IL-1 $\beta$ , IL-6, RANKL, and OPG protein concentrations were fitted simultaneously, and the resulting parameters were fixed and applied to fit the TRACP-5b and BMD data.

### Dynamics of IL-1 $\beta$ and IL-6 proteins

In the Earp model, mRNA concentration-time profiles of cytokines IL-1 $\beta$  and IL-6 after arthritis induction were well described by a series of transduction compartments with incorporation of the effects of bound CST-GR complex in the nucleus (DR<sub>N</sub>) and the remission compartment (Rem) (Earp et al. 2008a,b). The protein concentrations of IL-1 $\beta$  and IL-6 are modeled here as catenary compartments following the IL-1 $\beta$  and IL-6 mRNA transduction process. The equations for fitting IL-1 $\beta$  and IL-6 protein concentration-time profiles in both CIA and DEX-treated CIA rats are as follows:

$$\begin{aligned} \frac{dIL-1\beta_P}{dt} &= kin_{2P} \cdot IL-1\beta_M \cdot S_2 - kin_{2P} \cdot \frac{IL-1\beta_{M0}}{IL-1\beta_{P0}} \cdot IL-1\beta_P, \\ IL-1\beta_P(0) &= IL-1\beta_{P0} \end{aligned} \quad (1)$$

$$\begin{aligned} \frac{dIL-6_P}{dt} &= kin_{3P} \cdot IL-6_M \cdot S_3 - kin_{3P} \cdot \frac{IL-6_{M0}}{IL-6_{P0}} \cdot IL-6_P, \\ IL-6_P(0) &= IL-6_{P0} \end{aligned} \quad (2)$$

where  $kin_{2P}$  and  $kin_{3P}$  represent the synthesis rates of IL-1 $\beta$  and IL-6 proteins (shown as  $kin_{IL-1\beta}$  and  $kin_{IL-6}$  in Fig. 1),  $S_2$  and  $S_3$  are the proportionality constants between the disease-stimulated IL-1 $\beta$  and IL-6 mRNAs and their protein concentrations,  $IL-1\beta_{M0}$  and  $IL-6_{M0}$  are the baseline mRNA concentrations, and  $IL-1\beta_{P0}$  and  $IL-6_{P0}$  are the baseline protein concentrations (determined by the average values in healthy rats). The elimination rates of IL-1 $\beta$  and IL-6 proteins (shown as  $kout_{IL-1\beta}$  and  $kout_{IL-6}$  in Fig. 1), are represented by  $kin_{2P} \cdot (IL-1\beta_{M0}/IL-1\beta_{P0})$  and  $kin_{3P} \cdot (IL-6_{M0}/IL-6_{P0})$ .

### Dynamics of the bone remodeling system in healthy rats

The RANKL and OPG concentration-time profiles were fitted in a model expanded from a bone turnover model proposed by Lemaire et al. to describe the interactions between osteoblasts and osteoclasts during bone remodeling (Lemaire et al. 2004). This model was developed based on the effects of PTH and TGF- $\beta$ , which are two

important mediators regulating calcium homeostasis and bone remodeling, and it incorporates the regulation of the RANK/RANKL/OPG pathway in osteoblast/osteoclast activities. The original model, when unaltered, can describe the steady state and relationships of all the components, including, responding osteoblasts (ROB, referred as "R" in the Lemaire model), active osteoblasts (AOB, referred as "B" in the Lemaire model), active osteoclasts (AOC, referred as "C" in the Lemaire model), RANKL, and OPG.

In our model, most parameters remain the same as in the Lemaire model, while some are modified to fit the experimental data. Under healthy conditions, the dynamics of ROB, AOB, AOC, RANKL, and OPG are described by

$$\frac{dROB}{dt} = D_R \cdot \pi_{TGF} - \frac{D_B}{\pi_{TGF}} \cdot ROB, \quad ROB(0) = ROB_0 \quad (3)$$

$$\frac{dAOB}{dt} = \frac{D_B}{\pi_{TGF}} \cdot ROB - k_B \cdot AOB, \quad AOB(0) = AOB_0 \quad (4)$$

$$\begin{aligned} \frac{dAOC}{dt} &= D_C \cdot \pi_{RANK} - D_A \cdot \pi_{TGF} \cdot AOC, \\ AOC(0) &= AOC_0 \end{aligned} \quad (5)$$

where  $D_R$  and  $D_C$  are the differentiation rate constants of osteoblast progenitors and osteoclast precursors, and  $k_B$  and  $D_A$  are elimination rate constants of active osteoblasts and osteoclasts.  $D_B$  is the product of a fixed proportion ( $f_0$ ) and the differentiation rate constant of responding osteoblasts ( $d_B$ ). The  $\pi_{TGF}$  and  $\pi_{RANK}$  are receptor occupancies of TGF- $\beta$  and RANK as given by

$$\pi_{TGF} = \frac{AOC + f_0 \cdot AOC^S}{AOC + AOC^S} \quad (6)$$

$$\pi_{RANK} = \frac{KL}{K} = \frac{k_3}{k_4} \cdot L \quad (7)$$

where  $AOC^S$  is half the concentration of active osteoclasts yielding maximum TGF- $\beta$  receptor occupancy,  $KL$  is the concentration of RANK-RANKL complex,  $K$  is the concentration of RANK, and  $k_3$  and  $k_4$  are the binding and dissociation rate constants of the RANK-RANKL complex. The equation for the pseudo steady-state concentrations of RANKL (L) and OPG (O) are as follows:

$$L = \frac{kin_L \cdot AOB}{1 + k_3/k_4 \cdot K + 1/K_d \cdot O} \quad (8)$$

$$O = \frac{kin_O}{k_O} \cdot ROB \quad (9)$$

where  $kin_L$  (shown as  $kin_{RANKL}$  in Fig. 1) is the production rate constant of RANKL,  $K_d$  is the equilibrium dissociation constant of the OPG-RANKL complex, and  $kin_O$  and  $k_O$  are the production and loss rate constants of OPG (shown as  $kin_{OPG}$  and  $kout_{OPG}$  in Fig. 1). In the Lemaire model, productions of RANKL and OPG are subject to PTH binding and are governed by PTH receptor occupancy ( $\pi_p$ ). Since experimental data for both RANKL and OPG were obtained in our study, we estimated their production rate constants. The use of one parameter ( $kin_L$  or  $kin_O$ ) is for simplicity and to minimize overparameterization. The  $K_d$  for the OPG-RANKL complex is used instead of separate binding and dissociation rate constants ( $k_2/k_1$ ) for the same purpose. Details of the derivations of equations 7-9 can be found in supporting information Data S1.

### Dynamics of the bone remodeling system in CIA rats

Under arthritic conditions, proinflammatory cytokines are stimulated and they can affect the bone turnover process via multiple pathways. The ultimate result of these effects is bone loss, with is a significant risk in RA. There are numerous reports in the literature studying the mechanisms by which TNF- $\alpha$ , IL-1 $\beta$ , and IL-6 disrupt the osteoblast/osteoclast balance in RA. We aimed to include those mechanisms that are most commonly recognized and test their suitability in explaining our experimental data. The relationships between the inflammatory cytokines and the important components in bone remodeling and the model that can best describe our data are delineated below.

TNF- $\alpha$  is often regarded as one of the dominant mediators in RA and is also a potent inducer for other cytokines (Karmakar *et al.* 2010). In bone remodeling, TNF- $\alpha$  has been shown to inhibit the differentiation and maturation of osteoblasts (Gilbert *et al.* 2000; Nanes 2003), and stimulate the formation and activity of osteoclasts through both RANKL-dependent and -independent pathways (Goldring 2002; Walsh *et al.* 2005). TNF- $\alpha$  can directly increase the numbers of osteoclast precursors through up-regulation of c-Fms expression (Yao *et al.* 2006), and promote osteoclast differentiation with IL-1 $\alpha$  (Kobayashi *et al.* 2000). It can induce the expression of RANKL in bone marrow cells (Wei *et al.* 2005) and activate RANKL signaling pathway (Lam *et al.* 2000).

IL-1 $\beta$  also stimulates the production of RANKL in bone. Some studies suggested that the regulation of IL-1 $\beta$  on RANKL expression may be downstream of the TNF- $\alpha$ -mediated bone destructive cascade (Wei *et al.* 2005;

Zwerina *et al.* 2007), but there are also other studies that suggested this mechanism is TNF- $\alpha$ -independent (Ma *et al.* 2004; Wei *et al.* 2005). In vitro evidence from Wei *et al.* indicated that expressions of IL-1 receptor 1 (IL-1R1) were up-regulated in osteoclast precursor cells after addition of TNF- $\alpha$ , and, in turn, IL-1 augmented the osteoclast differentiation via the RANKL pathway. On the other hand, in IL-1R1 deficient mice, administration of TNF- $\alpha$  resulted in around 50% reduction in osteoclastogenesis, suggesting TNF- $\alpha$  can mediate this process without IL-1 $\beta$  (Wei *et al.* 2005). IL-1 $\beta$  has also been shown to have a direct stimulatory effect on osteoclasts (Goldring 2002; Walsh *et al.* 2005; Lorenzo *et al.* 2008). In the absence of osteoblasts, IL-1 can induce the maturation and bone-resorbing activity of osteoclasts (Jimi *et al.* 1999).

IL-6 has been shown to regulate bone resorption via the differentiation and maturation of osteoclasts (Goldring 2002; Lorenzo *et al.* 2008), and this may be mediated in a RANKL-independent manner (Kudo *et al.* 2003). Its effect on the RANKL-mediated pathway is controversial. Some studies suggested that it directly or indirectly induces RANKL expression (Palmqvist *et al.* 2002; Hashizume *et al.* 2008), but there are also studies that had contradictory results (Braun and Zwerina 2011; Suzuki *et al.* 2011). Liu *et al.* investigated the crosstalk between IL-6 and prostaglandin E<sub>2</sub> (PGE<sub>2</sub>) signaling pathways and how they govern osteoclastogenesis (Liu *et al.* 2005), and found that IL-6 participated in cyclooxygenase (COX)-2 mediated PGE<sub>2</sub> synthesis, which can promote osteoclast production though inhibition of OPG and stimulation of RANKL. There is also a positive feedback mechanism between PGE<sub>2</sub> and IL-6 in bone, by which one can augment the secretion of the other. The results of the Liu study also suggested that IL-6/PGE<sub>2</sub>-mediated osteoclastogenesis is mainly via the blockade of OPG production, whereas the increase in RANKL expression is minimal.

Since DEX is a potent immunosuppressant and is effective in eliciting a broad array of immune responses, it is difficult to differentiate its specific effects on bone remodeling apart from the suppression it causes in cytokines. It is well known that prolonged use of DEX and other glucocorticoids cause bone loss and fractures (Cooper *et al.* 1995), but its exact mechanism is not clear. Studies have suggested that DEX may directly or indirectly stimulate the production of osteoclasts via the RANKL pathway (Auphan *et al.* 1995), and prevent apoptosis of osteoclasts (Weinstein *et al.* 2002; Kim *et al.* 2006). Although the lifespan and number of osteoclasts may be increased by DEX, it suppresses the bone-resorbing activity of osteoclasts (Kim *et al.* 2006). The reduction in bone-resorbing activity is likely due to the disruption of the osteoclast cytoskeleton mediated by a macrophage colony-stimulating factor (M-CSF)-dependent pathway (Kim *et al.* 2006).

The final effect of DEX on BMD in CIA rats is essentially the result of these complicated interactions.

Taking all of these findings into consideration, the selected model was constructed with the change in each cytokine or DR<sub>N</sub> from its baseline affecting the components in the Lemaire model. It should be noted in the model, TNF- $\alpha$  (TNF- $\alpha_M$ ) represents mRNA concentrations as described in the Earp et al. article, whereas IL-1 $\beta$  (IL-1 $\beta_P$ ) and IL-6 (IL-6<sub>P</sub>) represent protein concentrations as described in equations 1 and 2. The equations are as follows:

$$L' = \frac{\text{kin}_L \cdot \text{AOB}'}{1 + k_3/k_4 \cdot K + 1/K_d \cdot O'} \cdot \left( 1 + \frac{S_{\text{max}_L}^{\text{TNF-}\alpha} \cdot (\text{TNF-}\alpha_M - \text{TNF-}\alpha_{M0})}{SC_{50_L}^{\text{TNF-}\alpha} + (\text{TNF-}\alpha_M - \text{TNF-}\alpha_{M0})} + \frac{S_{\text{max}_L}^{\text{IL-1}\beta} \cdot (\text{IL-1}\beta_P - \text{IL-1}\beta_{P0})}{SC_{50_L}^{\text{IL-1}\beta} + (\text{IL-1}\beta_P - \text{IL-1}\beta_{P0})} \right) \quad (15)$$

$$\begin{aligned} \frac{d\text{ROB}'}{dt} &= D_R \cdot \pi_{\text{TGF}' } \\ &\cdot \left( 1 - \frac{(\text{TNF-}\alpha_M - \text{TNF-}\alpha_{M0})}{IC_{50_R}^{\text{TNF-}\alpha} + (\text{TNF-}\alpha_M - \text{TNF-}\alpha_{M0})} \right) \\ &- \frac{D_B}{\pi_{\text{TGF}' }} \cdot \text{ROB}', \\ \text{ROB}'(0) &= \text{ROB}_0 \end{aligned} \quad (10)$$

$$\frac{d\text{AOB}' }{dt} = \frac{D_B}{\pi_{\text{TGF}' }} \cdot \text{ROB}' - k_B \cdot \text{AOB}', \quad \text{AOB}'(0) = \text{AOB}_0 \quad (11)$$

$$\begin{aligned} \frac{d\text{AOC}' }{dt} &= D_C \cdot \pi_{\text{RANK}' } \cdot \left( 1 + \frac{S_{\text{max}_C}^{\text{TNF-}\alpha} \cdot (\text{TNF-}\alpha_M - \text{TNF-}\alpha_{M0})}{SC_{50_C}^{\text{TNF-}\alpha} + (\text{TNF-}\alpha_M - \text{TNF-}\alpha_{M0})} + \frac{S_{\text{max}_C}^{\text{IL-1}\beta} \cdot (\text{IL-1}\beta_P - \text{IL-1}\beta_{P0})}{SC_{50_C}^{\text{IL-1}\beta} + (\text{IL-1}\beta_P - \text{IL-1}\beta_{P0})} \right) \\ &+ \frac{S_{\text{max}_C}^{\text{IL-6}} \cdot (\text{IL-6}_P - \text{IL-6}_{P0})}{SC_{50_C}^{\text{IL-6}} + (\text{IL-6}_P - \text{IL-6}_{P0})} \Big) - D_A \cdot \pi_{\text{TGF}' } \cdot \text{AOC}' \cdot \left( 1 - \frac{I_{\text{max}_C}^{\text{DRN}} \cdot (\text{DR}_N - \text{DR}_{N0})}{IC_{50_C}^{\text{DRN}} + (\text{DR}_N - \text{DR}_{N0})} \right), \text{AOC}'(0) = \text{AOC}_0 \end{aligned} \quad (12)$$

where ROB', AOB', and AOC' are the concentrations of responding osteoblasts, active osteoblasts, and active osteoclasts after CIA induction, IC<sub>50R</sub><sup>TNF- $\alpha$</sup>  is the sensitivity constant of the inhibition by TNF- $\alpha$  on osteoblast production, S<sub>maxC</sub><sup>TNF- $\alpha$</sup> , S<sub>maxC</sub><sup>IL-1 $\beta$</sup>  and S<sub>maxC</sub><sup>IL-6</sup> reflect stimulation of production of osteoclasts by cytokines TNF- $\alpha$ , IL-1 $\beta$ , and IL-6, while SC<sub>50C</sub><sup>TNF- $\alpha$</sup> , SC<sub>50C</sub><sup>IL-1 $\beta$</sup> , and SC<sub>50C</sub><sup>IL-6</sup> are the respective sensitivity constants, and I<sub>maxC</sub><sup>DRN</sup> and IC<sub>50C</sub><sup>DRN</sup> are the parameters regarding the effect of DR<sub>N</sub> on osteoclast apoptosis.

Receptor occupancies ( $\pi_{\text{TGF}'}$  and  $\pi_{\text{RANK}'}$ ), RANKL (L'), and OPG (O') in CIA rats were modeled as follows:

$$\pi_{\text{TGF}' } = \frac{\text{AOC}' + f_0 \cdot \text{AOC}^S}{\text{AOC}' + \text{AOC}^S} \quad (13)$$

$$\pi_{\text{RANK}' } = \frac{k_3}{k_4} \cdot L' \quad (14)$$

$$O' = \frac{\text{kin}_O}{k_O} \cdot \text{ROB}' \cdot \left( 1 - \frac{(\text{IL-6}_P - \text{IL-6}_{P0})}{IC_{50_O}^{\text{IL-6}} + (\text{IL-6}_P - \text{IL-6}_{P0})} \right) \quad (16)$$

where S<sub>maxL</sub><sup>TNF- $\alpha$</sup>  and S<sub>maxL</sub><sup>IL-1 $\beta$</sup>  reflect the stimulation of RANKL production by TNF- $\alpha$  and IL-1 $\beta$ , SC<sub>50L</sub><sup>TNF- $\alpha$</sup>  and SC<sub>50L</sub><sup>IL-1 $\beta$</sup>  are sensitivity constants, and IC<sub>50O</sub><sup>IL-6</sup> is the sensitivity constant for inhibition of OPG production by IL-6.

### Dynamics of TRACP-5b

TRACP-5b is derived from osteoclasts and is a marker for bone resorption (Halleen et al. 2000). In our model, TRACP-5b concentrations are linked to active osteoclasts (AOC), by which the ratio change controls the progres-

sion of TRACP-5b. The equation for TRACP-5b in CIA rats and its temporal changes after DEX is as follows:

$$\begin{aligned} \frac{d\text{TRACP-5b}}{dt} &= \text{kin}_T \cdot \left( \frac{\text{AOC}' }{\text{AOC}_0} \right) \gamma_C \\ &\cdot \left( 1 - \frac{I_{\text{max}_T}^{\text{DRN}} \cdot (\text{DR}_N - \text{DR}_{N0})^{\gamma_{DT}}}{(IC_{50_T}^{\text{DRN}})^{\gamma_{DT}} + (\text{DR}_N - \text{DR}_{N0})^{\gamma_{DT}}} \right) \\ &- \frac{\text{kin}_T}{\text{TRACP-5b}_0} \cdot (\text{TRACP-5b}), \\ \text{TRACP-5b}(0) &= \text{TRACP-5b}_0 \end{aligned} \quad (17)$$

where  $kin_T$  is the production rate constant of TRACP-5b (shown as  $kin_{TRACP5b}$  in Fig. 1),  $\gamma_C$  is the amplification factor  $I_{maxT}^{DRN}$ , and  $IC_{50T}^{DRN}$  are the capacity and sensitivity constants for inhibition of TRACP-5b by  $DR_N$ , and  $\gamma_{DT}$  is the Hill function for the inhibition. The elimination process ( $kout_T$ , shown as  $kout_{TRACP5b}$  in Fig. 1) is given by  $(kin_T)/$  (TRACP-5b<sub>0</sub>). TRACP-5b<sub>0</sub> is the baseline concentration and is the average value in healthy rats.

### Dynamics of bone mineral density

Bone mineral density (BMD) data were obtained previously (Earp et al. 2008a,b). BMD is determined by the balance between osteoblasts and osteoclasts. In our model, the production of bone turnover is linked to the ratio change in active osteoblasts (AOB), and the bone breakdown process is connected to the ratio change in active osteoclasts (AOC). Since the model was built to describe the whole bone system at the steady state, the profiles of AOB and AOC in healthy rats are flat and the ratio changes remain 1. Thus, in healthy animals the effect of AOB or AOC on BMD is not turned on and the equations are as follows:

$$\begin{aligned} \frac{dBMD_{LR}}{dt} &= kin_{LR} - \frac{kin_{LR}}{BMD_{LR0}} \cdot (BMD_{LR}) \\ &+ k_{grow} \cdot BMD_{LR} \cdot \left(1 - \frac{BMD_{LR}}{BMD_{LRSS}}\right), \quad (18) \\ BMD_{LR}(0) &= BMD_{LR0} \end{aligned}$$

$$\begin{aligned} \frac{dBMD_{TF}}{dt} &= kin_{TF} - \frac{kin_{TF}}{BMD_{TF0}} \cdot (BMD_{TF}) \\ &+ k_{grow} \cdot BMD_{TF} \cdot \left(1 - \frac{BMD_{TF}}{BMD_{TFSS}}\right), \quad (19) \\ BMD_{TF}(0) &= BMD_{TF0} \end{aligned}$$

$$\begin{aligned} \frac{dBMD_{DF}}{dt} &= kin_{DF} - \frac{kin_{DF}}{BMD_{DF0}} \cdot (BMD_{DF}) \\ &+ k_{grow} \cdot BMD_{DF} \cdot \left(1 - \frac{BMD_{DF}}{BMD_{DFSS}}\right), \quad (20) \\ BMD_{DF}(0) &= BMD_{DF0} \end{aligned}$$

$$\begin{aligned} \frac{dBMD_{MF}}{dt} &= kin_{MF} - \frac{kin_{MF}}{BMD_{MF0}} \cdot (BMD_{MF}) \\ &+ k_{grow} \cdot BMD_{MF} \cdot \left(1 - \frac{BMD_{MF}}{BMD_{MFSS}}\right), \quad (21) \\ BMD_{MF}(0) &= BMD_{MF0} \end{aligned}$$

$$\begin{aligned} \frac{dBMD_{EF}}{dt} &= kin_{EF} - \frac{kin_{EF}}{BMD_{EF0}} \cdot (BMD_{EF}) \\ &+ k_{grow} \cdot BMD_{EF} \cdot \left(1 - \frac{BMD_{EF}}{BMD_{EFSS}}\right), \quad (22) \\ BMD_{EF}(0) &= BMD_{EF0} \end{aligned}$$

A logistic function was used in each bone region to describe the natural growth (with rate constant  $k_{grow}$ ) of the bone. Parameters  $kin_{LR}$ ,  $kin_{TF}$ ,  $kin_{DF}$ ,  $kin_{MF}$ , and  $kin_{EF}$  are the production rate constants of lumbar vertebrae regions 1–4 (LR), total femur (TF), diaphyseal femur (DF), metaphyseal femur (MF), and epiphyseal femur (EF). The  $BMD_{LR0}$ ,  $BMD_{TF0}$ ,  $BMD_{DF0}$ ,  $BMD_{MF0}$ , and  $BMD_{EF0}$  are the baseline values of BMD in the respective regions, and  $BMD_{LRSS}$ ,  $BMD_{TFSS}$ ,  $BMD_{DFSS}$ ,  $BMD_{MFSS}$ , and  $BMD_{EFSS}$  are the steady-state BMD values at the end of the experiment.

For CIA rats, the ratio changes of AOB and AOC during natural disease progression and after DEX are incorporated in the equations as follows:

$$\begin{aligned} \frac{dBMD_{LR'}}{dt} &= kin_{LR} \cdot \left(\frac{AOB'}{AOB_0}\right)^{\gamma_{B_{LR}}} \\ &- \frac{kin_{LR}}{BMD_{LR0}} \cdot (BMD_{LR'}) \cdot \left(\frac{AOC'}{AOC_0}\right)^{\gamma_{C_{LR}}} \\ &+ k_{grow} \cdot BMD_{LR'} \cdot \left(1 - \frac{BMD_{LR'}}{BMD_{LRSS}}\right), \quad (23) \\ BMD_{LR'}(0) &= BMD_{LR0} \end{aligned}$$

$$\begin{aligned} \frac{dBMD_{TF'}}{dt} &= kin_{TF} \cdot \left(\frac{AOB'}{AOB_0}\right)^{\gamma_{B_{TF}}} \\ &- \frac{kin_{TF}}{BMD_{TF0}} \cdot (BMD_{TF'}) \cdot \left(\frac{AOC'}{AOC_0}\right)^{\gamma_{C_{TF}}} \\ &+ k_{grow} \cdot BMD_{TF'} \cdot \left(1 - \frac{BMD_{TF'}}{BMD_{TFSS}}\right), \quad (24) \\ BMD_{TF'}(0) &= BMD_{TF0} \end{aligned}$$

$$\begin{aligned} \frac{dBMD_{DF'}}{dt} &= kin_{DF} \cdot \left(\frac{AOB'}{AOB_0}\right)^{\gamma_{B_{DF}}} \\ &- \frac{kin_{DF}}{BMD_{DF0}} \cdot (BMD_{DF'}) \cdot \left(\frac{AOC'}{AOC_0}\right)^{\gamma_{C_{DF}}} \\ &+ k_{grow} \cdot BMD_{DF'} \cdot \left(1 - \frac{BMD_{DF'}}{BMD_{DFSS}}\right), \quad (25) \\ BMD_{DF'}(0) &= BMD_{DF0} \end{aligned}$$

$$\begin{aligned} \frac{dBMD_{MF'}}{dt} &= kin_{MF'} \cdot \left(\frac{AOB'}{AOB_0}\right)^{\gamma_{B_{MF}}} \\ &\quad - \frac{kin_{MF'}}{BMD_{MF0}} \cdot (BMD_{MF'}) \cdot \left(\frac{AOC'}{AOC_0}\right)^{\gamma_{C_{MF}}} \\ &\quad + k_{grow} \cdot BMD_{MF'} \cdot \left(1 - \frac{BMD_{MF'}}{BMD_{MFSS}}\right), \\ BMD_{MF'}(0) &= BMD_{MF0} \end{aligned} \tag{26}$$

$$\begin{aligned} \frac{dBMD_{EF'}}{dt} &= kin_{EF'} \cdot \left(\frac{AOB'}{AOB_0}\right)^{\gamma_{B_{EF}}} \\ &\quad - \frac{kin_{EF'}}{BMD_{EF0}} \cdot (BMD_{EF'}) \cdot \left(\frac{AOC'}{AOC_0}\right)^{\gamma_{C_{EF}}} \\ &\quad + k_{grow} \cdot BMD_{EF'} \cdot \left(1 - \frac{BMD_{EF'}}{BMD_{EFSS}}\right), \\ BMD_{EF'}(0) &= BMD_{EF0} \end{aligned} \tag{27}$$

where  $\gamma_{B_{LR}}$ ,  $\gamma_{B_{TF}}$ ,  $\gamma_{B_{DF}}$ ,  $\gamma_{B_{MF}}$ , and  $\gamma_{B_{EF}}$  are the amplification factors of the effects of AOB on the production of BMD in the five bone regions, and  $\gamma_{C_{LR}}$ ,  $\gamma_{C_{TF}}$ ,  $\gamma_{C_{DF}}$ ,  $\gamma_{C_{MF}}$ , and  $\gamma_{C_{EF}}$  are the amplification factors of the effects of AOC on the loss of BMD in the respective bone regions. This portion of the model resembles the equation used previously to model the progression of lumbar spine BMD in humans after treatment with denosumab (Peterson and Riggs 2012).

### Model fitting and data analysis

The area under the effect curves (AUEC) of concentration-time profiles of the IL-1 $\beta$ , IL-6, RANKL, OPG, and TRACP-5b in healthy, CIA, and DEX-dosed CIA rats were statistically compared by the two-sided Bailer-Satterthwaite method (Bailer 1988; Nedelman et al. 1995), and the t-statistic was calculated as follows:

$$t_{obs} = \frac{AUEC_C - AUEC_A}{\sqrt{s^2(AUEC_C) + s^2(AUEC_A)}} \tag{28}$$

where AUEC<sub>C</sub> and AUEC<sub>A</sub> are the AUEC of the control rats and CIA rats, and  $s^2(AUEC)$  is the variance of the AUEC. The profiles were considered statistically different if  $t_{obs} \geq 2.58$ , which is the Bonferroni-corrected critical value ( $z_{crit}$ ) in this analysis.

Model fittings were performed by nonlinear regression analysis using the maximum likelihood algorithm in the ADAPT 5 program (D'Argenio et al. 2009). Profiles of natural disease progression and all DEX dosing groups were fitted simultaneously and data from all the animals were naïve-pooled. The IL-1 $\beta$ , IL-6, RANKL, and OPG protein concentration-time profiles were fitted first, and the resulting parameters were fixed and applied to fit the TRACP-5b and BMD data. The variance model used is as follows:

$$V_i = (\sigma_1 + \sigma_2 \cdot Y_i)^2 \tag{29}$$

where  $V_i$  represents the variance of the  $i$ th data point,  $\sigma_1$  and  $\sigma_2$  are variance model parameters, and  $Y_i$  is the  $i$ th model prediction. A separate variance model was applied for each biomarker or disease endpoint. The final model was selected based on the success of minimization, modeling fittings, and reasonability and precision of parameter estimation.

## Results

### Measurements of protein concentrations in paw extracts

Our initial interest was to measure the protein concentrations of the three cytokines assessed in the Earp model (TNF- $\alpha$ , IL-1 $\beta$ , and IL-6) and incorporate them into the current model. We successfully measured and implemented the profiles of IL-1 $\beta$  and IL-6 protein concentrations in rat paws. However, preliminary experiments showed that the TNF- $\alpha$  protein concentration was not

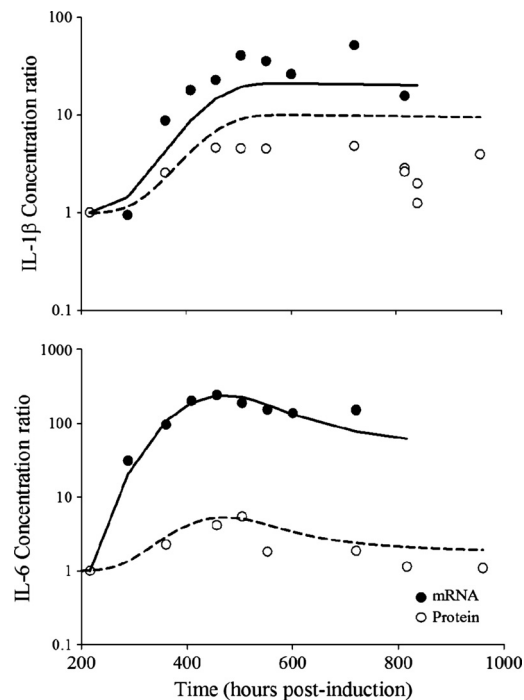


**Figure 2.** Disease progression of IL-1 $\beta$  and IL-6 mRNA and protein concentrations in CIA rats. Mean mRNA and protein concentrations at each time points were normalized with their respective baseline concentrations obtained on the first sacrifice time (day 9, 216 h post-induction). Solid and open circles depict normalized mRNA and protein profiles, and accompanying lines are normalized model predictions.

detectable, and hence it was not included in our model development. Instead, mRNA concentrations of TNF- $\alpha$  was included in the modeling analysis of this study.

### Dynamics of IL-1 $\beta$ and IL-6 proteins

Comparison of IL-1 $\beta$  and IL-6 mRNA and protein disease progression profiles is shown in Figure 2. The cytokine mRNA profiles were adopted from our previous

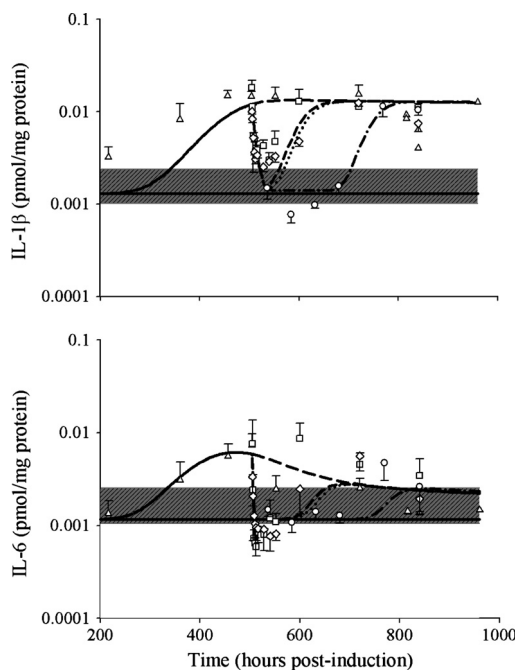


**Figure 3.** Disease progression and PD of DEX for IL-1 $\beta$  and IL-6 protein concentrations in CIA rats. The gray areas indicate the range of baseline concentrations (mean  $\pm$  SD) in healthy animals. Symbols and lines depict data from CIA control ( $\Delta$ , long dashed line), CIA receiving single 0.225 mg kg $^{-1}$  dose ( $\square$ , short dashed line), CIA receiving single 2.25 mg kg $^{-1}$  dose ( $\diamond$ , dotted line), and CIA receiving chronic doses of 0.225 mg kg $^{-1}$  groups ( $\circ$ , long dashed-dotted line). Model predictions for the respective groups are depicted by accompanying lines. CIA, collagen-induced arthritic; DEX, dexamethasone; PD, pharmacodynamic.

study (Earp et al. 2008b). It appeared that the mRNA and protein concentration profiles for both IL-1 $\beta$  and IL-6 correlated well, and the disease-state stimulation of mRNA was much higher than for the protein products. The disease onset times for mRNA and protein were similar, and the protein profiles of both cytokines generally followed the tendencies of their mRNA expressions (Earp et al. 2008b), where the concentration reached a steady state for IL-1 $\beta$ , and rose and fell off for IL-6 after disease onset.

Figure 3 depicts the profiles of IL-1 $\beta$  and IL-6 proteins in rat paws during CIA natural disease progression and DEX dosing. DEX caused a rapid drop in the protein concentrations of both cytokines in a manner similar to its effects to mRNA (Earp et al. 2008a). Chronic DEX effectively suppressed both cytokines to their baseline concentrations during the dosing period and the profiles returned to predose state after dosing is terminated.

Comparisons of AUEC revealed that CIA rats had significantly higher expressions of IL-1 $\beta$  (7.47 pmol mg $_{protein}^{-1}$  h) and IL-6 (2.11 pmol mg $_{protein}^{-1}$  h) than in healthy rats (1.06 and 1.17 pmol mg $_{protein}^{-1}$  h). After dosing, the AUEC of IL-1 $\beta$  in CIA rats receiving single 0.225 mg kg $^{-1}$ , single 2.25 mg kg $^{-1}$ , and chronic 0.225 mg kg $^{-1}$  SC DEX are 3.41, 2.57, and 1.52 pmol mg $_{protein}^{-1}$  h and were statistically lower than in CIA control rats and were significantly different from each other. For IL-6, the AUECs after dosing were 1.56, 1.09, and 0.704 pmol mg $_{protein}^{-1}$  h, respectively. The chronic dosing group exhibited significantly lower IL-6 than the CIA control and single-dose groups. No difference was found between the CIA control and CIA single-dose rats for IL-6.

The proposed model provided reasonable fittings of the profiles of both cytokines in CIA natural disease progression and under DEX dosing (Figs. 2, 3). There was a slight underestimation of protein concentrations of IL-1 $\beta$  during the rising phase in the CIA rats, (Fig. 3), which corresponds to the overestimation at the plateau phase in the normalized profiles in Figure 2. However, it was

**Table 1.** Model parameter estimates for the dynamics of IL-1 $\beta$  and IL-6 proteins.

Parameter (Units)	Definition	Estimate	CV %
$kin_{2P}$ (pmol h $^{-1}$ nmol $_{mRNA}^{-1}$ )	Synthesis rate constant for IL-1 $\beta$ protein	$3.94 \times 10^{-5}$	7.45
$S_2$	Proportionality constant of disease-stimulated IL-1 $\beta$ mRNA and protein	0.454	0.674
IL-1 $\beta$ $_{P0}$ (pmol mg $_{protein}^{-1}$ )	IL-1 $\beta$ protein baseline	0.00129	FIXED
$kin_{3P}$ (pmol h $^{-1}$ nmol $_{mRNA}^{-1}$ )	Synthesis rate constant for IL-6 protein	$1.63 \times 10^{-4}$	38.2
$S_3$	Proportionality constant of disease-stimulated IL-6 mRNA and protein	0.00332	5.33
IL-6 $_{P0}$ (pmol mg $_{protein}^{-1}$ )	IL-6 protein baseline	0.00116	FIXED

CV %, coefficient of variation.

acceptable, given that there are considerable variabilities among the CIA animals and the plateau phase was adequately captured. The parameter estimates for IL-1 $\beta$  and IL-6 proteins are listed in Table 1. The synthesis rate constants for IL-1 $\beta$  and IL-6 were  $3.94 \times 10^{-5}$  and  $1.63 \times 10^{-4}$  pmol mg<sub>protein</sub><sup>-1</sup> h<sup>-1</sup> nmol<sub>mRNA</sub><sup>-1</sup>, reflecting the slow translation process from mRNA to protein. The proportionality constants ( $S_2$  and  $S_3$ ) between mRNA and protein concentrations for IL-1 $\beta$  and IL-6 were 0.454 and 0.00332.

### Dynamics of the bone remodeling system

The predicted profiles of ROB, AOB, and AOC under healthy and CIA conditions are presented in Figure 4. In healthy animals, ROB, AOB, and AOC are at homeostasis and the model predictions showed that the profiles of the three components remained flat throughout the study

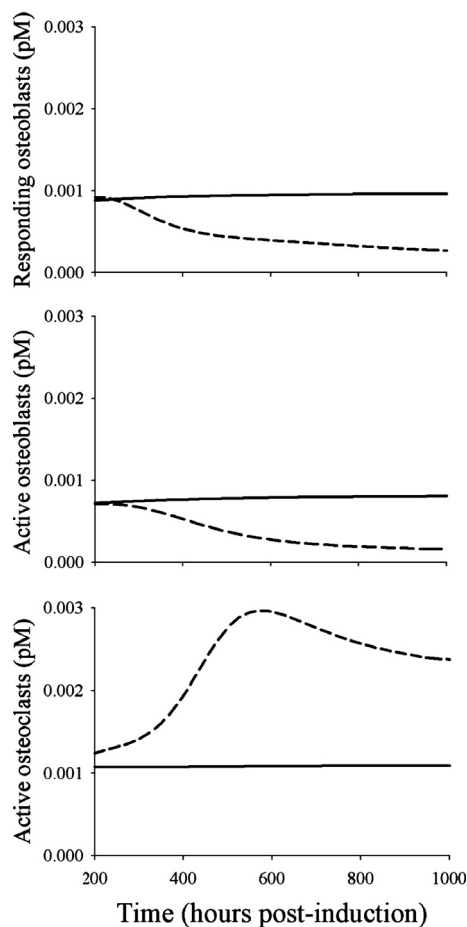


**Figure 4.** Model predicted concentration-time profiles of responding osteoblasts, active osteoblasts, and active osteoclasts under healthy (solid lines) and CIA disease (long dashed lines) conditions. CIA, collagen-induced arthritic.

period. Under the arthritic conditions, the simulations indicated that both ROB and AOB gradually declined and reached new steady states, whereas AOC demonstrated a rise and fall profile similar to IL-6.

Figure 5 shows the disease progression and PD of DEX for RANKL and OPG proteins. The profile of RANKL disease progression in CIA rats exhibited a similar pattern to IL-6, where it rose around day 14 (336 h) post-induction, peaked at around day 21 (504 h), and then gradually declined. Analysis of AUEC showed that RANKL was significantly higher in CIA rats (4.10 pmol mg<sub>protein</sub><sup>-1</sup> h) than in healthy rats (1.25 pmol mg<sub>protein</sub><sup>-1</sup> h). DEX rapidly decreased RANKL expression after administration, and there was a small rebound of RANKL concentration after dosing ceased. Chronic DEX caused a sustained suppression of RANKL during the dosing period, and the reduction caused RANKL to drop below the baseline concentration (as shown in Fig. 5). Postdose

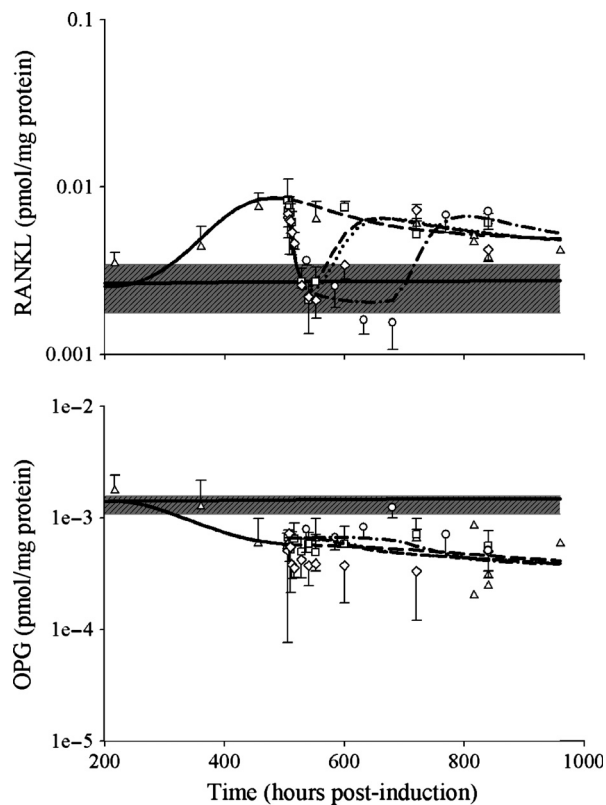


**Figure 5.** Disease progression and PD of DEX for RANKL and OPG protein concentrations in CIA rats. The gray areas indicate the range of baseline concentrations (mean  $\pm$  SD) in healthy animals. Symbols and lines depict data from CIA control ( $\Delta$ , long dashed line), CIA receiving single  $0.225 \text{ mg kg}^{-1}$  dose ( $\square$ , short dashed line), CIA receiving single  $2.25 \text{ mg kg}^{-1}$  dose ( $\diamond$ , dotted line), and CIA receiving chronic doses of  $0.225 \text{ mg kg}^{-1}$  groups ( $\circ$ , long dashed-dotted line). CIA, collagen-induced arthritic; DEX, dexamethasone; PD, pharmacodynamic; OPG, osteoprotegerin.

**Table 2.** Model parameter estimates for the bone remodeling system.

Parameter (Units)	Definition	Estimate	CV %
$D_R$ (pmol L <sup>-1</sup> h <sup>-1</sup> )	Differentiation rate of osteoblast progenitors	$2.92 \times 10^{-5}$	FIXED
$f_0$	Fixed proportion	0.05	FIXED
AOC <sup>s</sup> (pmol L <sup>-1</sup> )	Value of C to get half differentiation flux	$5 \times 10^{-3}$	FIXED
$d_B$ (h <sup>-1</sup> )	Differentiation rate of responding osteoblasts	0.0292	FIXED
$k_B$ (h <sup>-1</sup> )	Elimination rate of active osteoblasts	$7.88 \times 10^{-3}$	FIXED
$k_3$ (pmol L <sup>-1</sup> h <sup>-1</sup> )	Rate of RANK-RANKL binding	$2.42 \times 10^{-5}$	FIXED
$k_4$ (h <sup>-1</sup> )	Rate of RANK-RANKL dissociation	$7.08 \times 10^{-4}$	FIXED
$k_O$ (h <sup>-1</sup> )	Elimination rate of OPG	0.0146	FIXED
$D_A$ (h <sup>-1</sup> )	Osteoclast apoptosis rate due to TGF- $\beta$	0.0292	FIXED
$K$ (pmol L <sup>-1</sup> )	Concentration of RANK	10	FIXED
ROB <sub>0</sub> (pmol L <sup>-1</sup> )	Responding osteoblast baseline	$7.73 \times 10^{-4}$	FIXED
AOB <sub>0</sub> (pmol L <sup>-1</sup> )	Active osteoblast baseline	$7.28 \times 10^{-4}$	FIXED
AOC <sub>0</sub> (pmol L <sup>-1</sup> )	Active osteoclast baseline	$9.13 \times 10^{-4}$	FIXED
$kin_L$ (pmol mg <sub>protein</sub> <sup>-1</sup> h <sup>-1</sup> pmol L <sup>-1</sup> )	Production rate constant of RANKL	46.5	73.8
$K_d$ (pmol mg <sub>protein</sub> <sup>-1</sup> )	Dissociation rate constant of RANKL-OPG	$1.21 \times 10^{-4}$	76.4
$kin_O$ (pmol mg <sub>protein</sub> <sup>-1</sup> h <sup>-1</sup> pmol L <sup>-1</sup> )	Production rate constant of OPG	0.0224	29.0
$D_C$ (pmol L <sup>-1</sup> h <sup>-1</sup> )	Differentiation rate of osteoclast precursors	0.0757	41.7
$S_{max}^{TNF-\alpha}$	Stimulation of RANKL via TNF	0.0554	130
$S_{max}^{IL-1\beta}$	Stimulation of osteoclasts via TNF	0.0231	327
$S_{max}^{IL-1\beta}$	Stimulation of RANKL via IL-1 $\beta$	4.57	28.9
$S_{max}^{IL-6}$	Stimulation of osteoclasts via IL-1 $\beta$	0.0198	122
$I_{max}^{DRN}$	Stimulation of osteoclasts via IL-6	0.0599	252
$I_{max}^{DRN}$	Inhibition of osteoclasts by DR <sub>N</sub>	0.423	46.0
$IC_{50}^{TNF-\alpha}$ (pmol mg <sub>RNA</sub> <sup>-1</sup> )	Sensitivity of TNF inhibition on osteoblasts	0.0138	45.7
$SC_{50}^{TNF-\alpha}$ (pmol mg <sub>RNA</sub> <sup>-1</sup> )	Sensitivity of TNF stimulation on RANKL	0.0659	234
$SC_{50}^{TNF-\alpha}$ (pmol mg <sub>RNA</sub> <sup>-1</sup> )	Sensitivity of TNF stimulation on osteoclasts	0.00425	485
$SC_{50}^{IL-1\beta}$ (pmol mg <sub>protein</sub> <sup>-1</sup> )	Sensitivity of IL-1 $\beta$ stimulation on RANKL	0.0137	49.6
$SC_{50}^{IL-1\beta}$ (pmol mg <sub>protein</sub> <sup>-1</sup> )	Sensitivity of IL-1 $\beta$ stimulation on osteoclasts	$7.20 \times 10^{-4}$	280
$SC_{50}^{IL-6}$ (pmol mg <sub>protein</sub> <sup>-1</sup> )	Sensitivity of IL-6 stimulation on osteoclasts	$7.02 \times 10^{-4}$	77.8
$IC_{50}^{IL-6}$ (pmol mg <sub>protein</sub> <sup>-1</sup> )	Sensitivity of IL-6 inhibition on OPG	0.0294	82.5
$IC_{50}^{DRN}$ (nmol L <sup>-1</sup> )	Sensitivity of DR <sub>N</sub> inhibition on osteoclasts	$5.49 \times 10^{-7}$	310

CV %, coefficient of variation; RANKL, receptor activator of nuclear factor kappa-B ligand; OPG, osteoprotegerin.

AUECs of RANKL were 1.86, 1.63, and 1.19 pmol mg<sup>-1</sup> protein<sup>-1</sup> h after single 0.225 mg kg<sup>-1</sup>, single 2.25 mg kg<sup>-1</sup>, and chronic 0.225 mg kg<sup>-1</sup> DEX, and statistical analyses showed that these are all significantly lower than CIA control rats. The AUEC values also differed among all the treatment groups.

OPG, as a decoy receptor of RANKL, showed an opposite profile compared to RANKL after CIA induction. At around the time (day 14 post-induction) that concentrations of cytokines and RANKL began to rise, OPG started to drop and then reached a new steady state around day 21 (504 h). This decrease is statistically significant with AUECs of 0.833 and 0.552 pmol mg<sub>protein</sub><sup>-1</sup> h for healthy and CIA rats. The effects of DEX on OPG disease progression appeared to be modest and no significant difference was revealed when comparing the AUEC of the CIA control rats with any of the dosing groups. However, there seemed to be a slightly increasing trend observed in the chronic dosing group (Fig. 5).

The parameter estimates of the system are listed in Table 2. All fixed parameters were adapted from the Lemaire model. The two parameters reflecting the activity of osteoblasts and osteoclasts that were estimated are  $K_d$  (dissociation rate constant of the RANKL-OPG complex) as  $1.21 \times 10^{-4}$  pmol mg<sub>protein</sub><sup>-1</sup> and  $D_C$  (differentiation rate of osteoclast precursors) as 0.0757 pmol L<sup>-1</sup> h<sup>-1</sup>. The estimate for the production rate constant of RANKL ( $kin_R$ ) was 46.5 pmol mg<sub>protein</sub><sup>-1</sup> h<sup>-1</sup> pmol L<sup>-1</sup> and was 0.0224 pmol mg<sub>protein</sub><sup>-1</sup> h<sup>-1</sup> pmol L<sup>-1</sup> for OPG ( $kin_O$ ). Estimates of  $S_{max}$  revealed that IL-1 $\beta$  (4.57) had a stronger effect on the production of RANKL than TNF- $\alpha$  (0.00554). The effect of IL-6 (0.0599) on the stimulation of osteoclasts was higher than both TNF- $\alpha$  (0.0231) and IL-1 $\beta$  (0.0198). Estimates of  $IC_{50}$  and  $SC_{50}$  suggested that all three cytokines had sensitive effects on osteoclasts. The  $SC_{50}$  of TNF- $\alpha$  on osteoclasts was 0.00425 pmol mg<sub>RNA</sub><sup>-1</sup>, which is lower than its effect on osteoblasts ( $IC_{50} = 0.0138$  pmol mg<sub>RNA</sub><sup>-1</sup>) and on RANKL ( $SC_{50} = 0.0659$  pmol

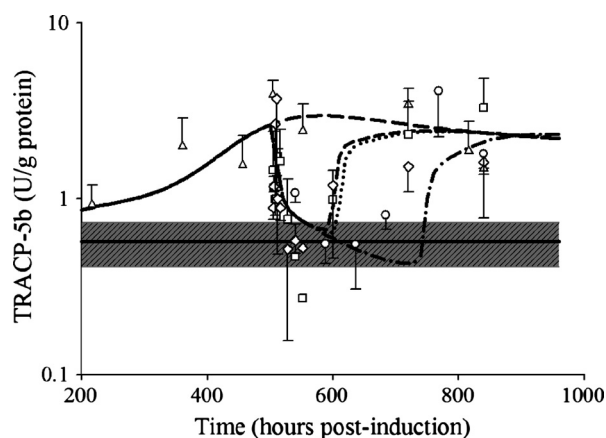


**Figure 6.** Disease progression and PD of DEX for TRACP-5b in CIA rats. The closed circles (●) depict healthy animals. The gray area indicates the range of baseline concentrations (mean  $\pm$  SD) in healthy animals. Symbols and lines depict data from CIA control ( $\Delta$ , long dashed line), CIA receiving single  $0.225 \text{ mg kg}^{-1}$  dose ( $\square$ , short dashed line), CIA receiving single  $2.25 \text{ mg kg}^{-1}$  dose ( $\diamond$ , dotted line), and CIA receiving chronic doses of  $0.225 \text{ mg kg}^{-1}$  groups ( $\circ$ , long dashed-dotted line). CIA, collagen-induced arthritic; DEX, dexamethasone; PD, pharmacodynamic; TRACP-5b, tartrate-resistant acid phosphatase 5b.

**Table 3.** Model parameter estimates for the dynamics of TRACP-5b.

Parameter (Units)	Definition	Estimate	CV %
$kin_T$ ( $\text{U L}^{-1} \text{h}^{-1}$ )	Synthesis rate constant for TRACP-5b	0.0918	34.6
TRACP-5 $\beta_0$ ( $\text{U L}^{-1}$ )	TRACP-5b baseline	0.570	FIXED
$\gamma_C$	Amplification factor of osteoclasts on TRACP-5b	1.38	4.31
$I_{max_T}^{DRN}$	Inhibition of TRACP-5b by $DR_N$	0.678	22.0
$IC_{50_T}^{DRN}$ ( $\text{nmol L}^{-1}$ )	Sensitivity constant of $DR_N$ inhibition on TRACP-5b	31.1	8.29
$\gamma_{DT}$	Hill function of the $DR_N$ inhibition on TRACP-5b	10	FIXED

CV %, coefficient of variation; TRACP-5b, tartrate-resistant acid phosphatase 5b.

$\text{mg}_{\text{RNA}}^{-1}$ ). The stimulation of IL-1 $\beta$  on osteoclasts ( $SC_{50} = 7.20 \times 10^{-4} \text{ pmol mg}_{\text{protein}}^{-1}$ ) was more sensitive than its effect on RANKL ( $SC_{50} = 0.0137 \text{ pmol mg}_{\text{protein}}^{-1}$ ). The sensitivity of IL-6 on osteoclasts was  $7.02 \times 10^{-4} \text{ pmol mg}_{\text{protein}}^{-1}$ , which is also much lower than its sensitivity on OPG inhibition ( $IC_{50} = 0.0294 \text{ pmol mg}_{\text{protein}}^{-1}$ ).

### Dynamics of TRACP-5b

Concentration-time profiles, the TRACP-5b, and predicted profiles of active osteoclasts (AOC) after DEX

dosing are shown in Figure 6. Disease progression of TRACP-5b after CIA induction exhibited a profile similar to that of RANKL or IL-6 and had the typical pattern of delay, rise to peak, and then fall off (Fig. 6). Statistical analysis indicated that the AUEC of TRACP-5b expression in CIA rats ( $1444 \text{ U g}_{\text{protein}}^{-1} \cdot \text{h}$ ) was significantly higher than in healthy rats ( $356 \text{ U g}_{\text{protein}}^{-1} \cdot \text{h}$ ). DEX dosing effectively decreased TRACP-5b concentrations, and all DEX dosing groups had a significantly lower AUEC ( $608$ ,  $433$ , and  $527 \text{ U g}_{\text{protein}}^{-1} \cdot \text{h}$  after single  $0.225 \text{ mg kg}^{-1}$ , single  $2.25 \text{ mg kg}^{-1}$ , and chronic  $0.225 \text{ mg kg}^{-1}$  doses) than the CIA control rats after drug administration at day 21. No differences were revealed among the DEX dosing groups.

Since TRACP-5b is a marker of bone resorption, it was of interest to compare its progression with that of the bone-resorbing osteoclasts. The proposed model assumed that DEX not only affected the apoptosis of osteoclasts (i.e.  $I_{max_C}^{DRN}$  and  $IC_{50_C}^{DRN}$ ), but also inhibited their activity (i.e.  $I_{max_T}^{DRN}$  and  $IC_{50_T}^{DRN}$ ) and hence decreased the production of TRACP-5b. Model fittings (Fig. 6) indicated that the model well captured the rapid drop of TRACP-5b concentrations after DEX, reflecting the suitability of this model to explain the PD of DEX on TRACP-5b disease progression. The parameter estimates are listed in Table 3. All parameters were estimated with good precision (low CV %). The maximum inhibition on TRACP-5b production by DEX ( $I_{max_T}^{DRN}$ ) was estimated to be 67.8%, with  $IC_{50_T}^{DRN}$  of  $31.1 \text{ nmol L}^{-1}$ .

### Dynamics of bone mineral density

The profiles of BMD in the five bone areas (lumbar vertebrae 1–4, total femur, diaphyseal femur, metaphyseal femur, and epiphyseal femur) are shown in Figure 7. In healthy rats, there were gradual increases in BMD of all five bone regions during the experiment period, and the logistic model well captured these behaviors. In CIA rats, bone loss began at around 420 h after disease induction, and BMD stayed low throughout the rest of experiment. DEX chronic dosing at  $0.225 \text{ mg kg}^{-1}$  did not seem to have strong protective effects against bone loss, and in most cases the profiles after DEX largely overlap with the natural disease progression profiles. By linking the bone formation process with the osteoblasts and the bone breakdown process with the osteoclasts, our proposed model could reasonably describe the BMD during disease progression and DEX effects in all five bone regions. Parameter estimates (in Table 4) showed that  $kin$  values for all bone regions have small values (about  $1 \times 10^{-4} \text{ g cm}^{-2} \text{ h}^{-1}$ ), reflecting the slow bone turnover process. The AOB and AOC appeared to have various degrees of contribution toward the five bone regions,

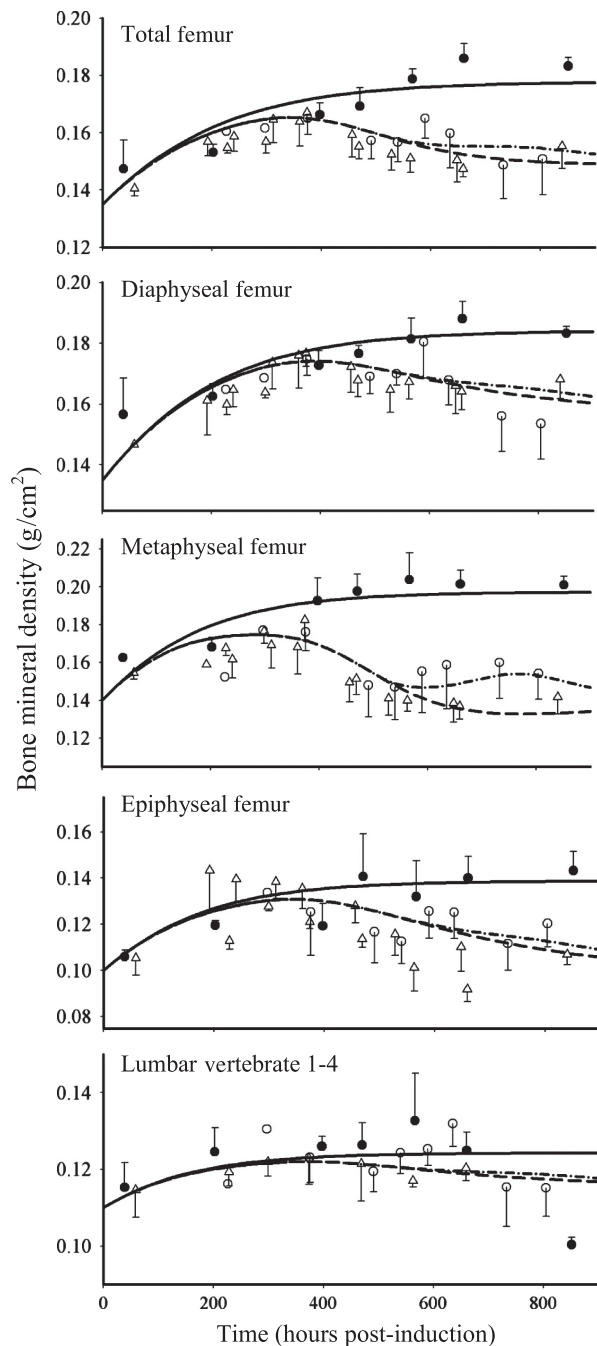


**Figure 7.** Profiles of BMD in different bone regions in healthy (●) and CIA rats. Symbols depict data from CIA control (Δ) and CIA rats receiving chronic doses of  $0.225 \text{ mg kg}^{-1}$  DEX (○). Lines depict model predictions in corresponding groups. BMD, bone mineral density; CIA, collagen-induced arthritic; DEX, dexamethasone; RANKL, receptor activator of nuclear factor kappa-B ligand.

which are reasonable considering the differences in their bone compositions. It is also interesting that the estimates of the amplification factors ( $\gamma_{B_{LR}} = 0.170$  and  $\gamma_{C_{LR}} = 0.0542$ ) for lumbar vertebrae 1-4 (LR) are

surprisingly close to the values reported by Peterson and Riggs for lumbar spine ( $\gamma_{OB} = 0.0739$  and  $\gamma_{OC} = 0.0679$ ) (Peterson and Riggs 2012).

## Discussion

In this study, we aimed to incorporate as many biomarkers as possible in order to construct a more comprehensive model for RA. We also attempted to measure TNF- $\alpha$  protein, but it could not be detected in the paws of either healthy or CIA rats. This is consistent with findings in a previous study (Stolina *et al.* 2008). The joint damage caused by TNF- $\alpha$  may be further mediated by IL-1 (Zwerina *et al.* 2007), where IL-1 augments the TNF- $\alpha$ -activated RANKL up-regulation (Walsh *et al.* 2005; Karmakar *et al.* 2010). Our model seemed to support these findings. The estimated sensitivity constants for RANKL induction were  $SC_{50L}^{TNF-\alpha} = 0.0659 \text{ pmol mg}_{RNA}^{-1}$  (4.40-fold from the baseline value  $0.0150 \text{ pmol mg}_{RNA}^{-1}$ ) for TNF- $\alpha$ , and  $SC_{50L}^{IL-1\beta} = 0.0137 \text{ pmol mg}_{protein}^{-1}$  (10.6-fold from the baseline value  $0.00129 \text{ pmol mg}_{protein}^{-1}$ ) for IL-1 $\beta$ . This indicated that TNF- $\alpha$  responded to RANKL activation faster than IL-1 $\beta$ . Our results also showed that the maximum effects on RANKL induction by TNF- $\alpha$  ( $S_{maxL}^{TNF-\alpha}$ ) and IL-1 $\beta$  ( $S_{maxL}^{IL-1\beta}$ ) were 0.0554 and 4.57, which is consistent with the findings that IL-1 $\beta$  was the main mediator for RANKL induction.

TNF- $\alpha$  appeared to be the most sensitive in its stimulation of osteoclast production ( $SC_{50C}^{TNF-\alpha} = 0.00425 \text{ pmol mg}_{RNA}^{-1}$ ) compared with its effects on osteoblasts ( $IC_{50R}^{TNF-\alpha} = 0.0138 \text{ pmol mg}_{RNA}^{-1}$ ) and RANKL ( $SC_{50L}^{TNF-\alpha} = 0.0659 \text{ pmol mg}_{RNA}^{-1}$ ), and this is true for both IL-1 $\beta$  and IL-6 as well. These results suggest that the immune cascade in RA primarily affects osteoclasts in the regulation of bone loss and emphasizes the importance of osteoclasts. Other studies also found that osteoclasts are the primary driver for bone loss in RA, whereas osteoblasts indirectly modulate the process (Walsh *et al.* 2005; Karmakar *et al.* 2010).

The disease progression of IL-1 $\beta$  and IL-6 proteins appeared consistent with previous studies (Stolina *et al.* 2008). It also appeared that their protein concentrations corresponded well with the mRNA profiles, which is consistent with the findings in a CIA mouse model (Rioja *et al.* 2004). The PD effects of DEX on IL-1 $\beta$  and IL-6 proteins resembled observations of their mRNA profiles, and such relationships allowed the use of a simple proportionality constant to link the mRNA and protein profiles. These suggested that IL-1 $\beta$  and IL-6 mRNAs are good surrogates for assessing the dynamics of their protein concentrations in CIA rats, and the assumptions which the Earp model applied were valid.

**Table 4.** Model parameter estimates for bone mineral density.

Parameter (Units)	Definition	Estimate	CV %
$k_{\text{grow}}$ (g cm <sup>-2</sup> h <sup>-1</sup> )	Natural growth rate of BMD	$5.43 \times 10^{-3}$	15.8
$L_0$ (g cm <sup>-2</sup> )	Lumbar vertebrae 1–4 initial BMD	0.110	FIXED
$TF_0$ (g cm <sup>-2</sup> )	Total femur initial BMD	0.135	FIXED
$DF_0$ (g cm <sup>-2</sup> )	Diaphyseal femur initial BMD	0.135	FIXED
$MF_0$ (g cm <sup>-2</sup> )	Metaphyseal femur initial BMD	0.140	FIXED
$EF_0$ (g cm <sup>-2</sup> )	Epiphyseal femur initial BMD	0.100	FIXED
$LR_{\text{ss}}$ (g cm <sup>-2</sup> )	Lumbar vertebrae 1–4 steady-state BMD	0.129	12.4
$TF_{\text{ss}}$ (g cm <sup>-2</sup> )	Total femur steady-state BMD	0.183	2.82
$DF_{\text{ss}}$ (g cm <sup>-2</sup> )	Diaphyseal femur steady-state BMD	0.195	7.13
$MF_{\text{ss}}$ (g cm <sup>-2</sup> )	Metaphyseal femur steady-state BMD	0.233	13.9
$EF_{\text{ss}}$ (g cm <sup>-2</sup> )	Epiphyseal femur steady-state BMD	0.162	20.9
$kin_{\text{LR}}$ (g cm <sup>-2</sup> h <sup>-1</sup> )	Production rate constant of lumbar vertebrae 1–4 BMD	$1.98 \times 10^{-4}$	360
$kin_{\text{TF}}$ (g cm <sup>-2</sup> h <sup>-1</sup> )	Production rate constant of total femur BMD	$8.24 \times 10^{-5}$	80.1
$kin_{\text{DF}}$ (g cm <sup>-2</sup> h <sup>-1</sup> )	Production rate constant of diaphyseal femur BMD	$1.54 \times 10^{-4}$	124
$kin_{\text{MF}}$ (g cm <sup>-2</sup> h <sup>-1</sup> )	Production rate constant of metaphyseal femur BMD	$4.05 \times 10^{-4}$	68.4
$kin_{\text{EF}}$ (g cm <sup>-2</sup> h <sup>-1</sup> )	Production rate constant of epiphyseal femur BMD	$2.83 \times 10^{-4}$	126
$\gamma_{\text{BLR}}$	Amplification factor of osteoblast on lumbar vertebrae	0.170	437
$\gamma_{\text{BTF}}$	Amplification factor of osteoblast on total femur	3.19	151
$\gamma_{\text{BDF}}$	Amplification factor of osteoblast on diaphyseal femur	1.02	293
$\gamma_{\text{BMF}}$	Amplification factor of osteoblast on metaphyseal femur	0.00643	37.3
$\gamma_{\text{BEF}}$	Amplification factor of osteoblast on epiphyseal femur	0.746	232
$\gamma_{\text{CLR}}$	Amplification factor of osteoclast on lumbar vertebrae	0.0542	480
$\gamma_{\text{CTF}}$	Amplification factor of osteoclast on total femur	0.528	136
$\gamma_{\text{CDF}}$	Amplification factor of osteoclast on diaphyseal femur	0.119	259
$\gamma_{\text{CMF}}$	Amplification factor of osteoclast on metaphyseal femur	0.588	46.0
$\gamma_{\text{CEF}}$	Amplification factor of osteoclast on epiphyseal femur	0.0827	225

CV %, coefficient of variation.

The disease progression profiles of RANKL and OPG in CIA rat paws agreed with previous findings, where the two progressed in the opposite direction and then reached the steady state as time proceeded (Stolina et al. 2008). In our study, RANKL:OPG ratios in CIA rats increased over time and remained elevated at the end of the study, which suggested the presence of active bone resorption. Our model assumptions about the cytokine regulation of RANKL, OPG, osteoblasts, and osteoclasts were all obtained from the literature, and the modeling results revealed that connecting these mechanisms together can adequately explain the progression of RANKL and OPG in RA and, surprisingly, also capture the PD effects of DEX dosing.

Our results regarding the disease progression profile of TRACP-5b confirmed the previous findings that TRACP-5b is significantly raised after disease onset slightly later than RANKL (Stolina et al. 2005). It was suggested that secreted TRACP-5b represents the number of osteoclasts (Alatalo et al. 2004; Rissanen et al. 2008). Thus, in our model, we first attempted to link the ratio changes of the AOC compartment directly to TRACP-5b, and it functioned well in describing its disease progression. However, DEX caused a much faster drop in TRACP-5b concentra-

tions than in the simulated AOC compartment, which suggested there may be undescribed inhibitory pathways. The inhibition described by Kim et al. regarding the DEX effect on osteoclast function was then applied to fit the data (Kim et al. 2006), and it appeared to capture the profiles of TRACP-5b well.

By incorporating the ratio changes of AOB and AOC into the formation and elimination processes of bone turnover, our modeling well captured CIA disease progression and DEX PD profiles of the BMD in all five bone regions. Although DEX could effectively suppress cytokine expressions, it appeared that it only had modest effects on BMD. This is likely because DEX can simultaneously modulate the activity of osteoblasts and osteoclasts, and it can shift the balance in both directions. This bidirectional nature is the reason why dosages and dosing regimens are critical for DEX monotherapy, and dose optimization is important for DEX therapy to attain therapeutic benefits and prevent bone loss.

We performed simulations to predict scenarios where individual mediators (IL-1 $\beta$ , IL-6, or RANKL) are completely inhibited (Fig. 8). The effect of inhibition of IL-1 $\beta$  or RANKL seems to be similar, resulting in comparable degree of improvement in the BMD profiles and RANKL:

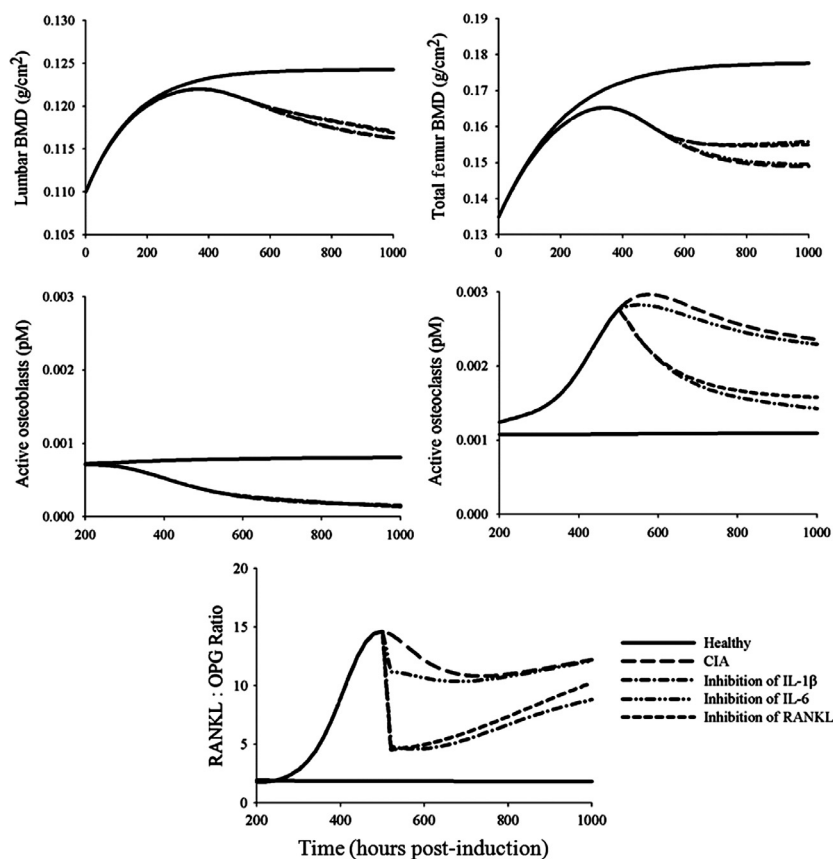


**Figure 8.** Model predictions of time profiles of lumbar BMD, total femur BMD, active osteoblasts, active osteoclasts, and the RANKL:OPG ratios under different potential therapeutic approaches. Therapeutic interventions were assumed to start at 504 h (21 days) post-induction and continue to 1000 h. Solid and long-dashed lines depict the profiles in healthy and CIA rats. Lines show profiles under complete inhibition of indicated agents. BMD, bone mineral density; CIA, collagen-induced arthritic; RANKL, receptor activator of nuclear factor kappa-B ligand; OPG, osteoprotegerin.

OPG ratios. On the contrary, inhibition of IL-6 appears to be the least effective in obviating bone loss. It was shown that tocilizumab (anti-IL-6 antibody) may induce OPG expression but not RANKL (Kanbe et al. 2012). Although this matches our model predictions, it is important to consider that the efficacy of anti-IL-6 therapy against bone loss may be related to the Wnt signaling pathway (Corrado et al. 2013), which was not included in our model. The efficacy of tocilizumab toward bone loss is likely to be resulted from both mechanisms.

It should be noted that there are limitations in our model. One caveat is that some assumptions may be oversimplified. An example is that simple additive relationships were assumed for processes where several mediators simultaneously come into effect. This might not be true considering the tight regulations among the cytokines. For instance, TNF- $\alpha$  and IL-1 may be synergistic for their induction of RANKL (Wei et al. 2005). Another point to keep in mind is the exclusion of other RA pathological pathways or signals in our model. We

assumed that effects of hormones PTH and TGF- $\beta$  on bone were minimal compared with cytokines in RA, and this is because most reports emphasize the roles of cytokines and there have been controversies regarding the roles of PTH (Af Ekenstam et al. 1990; Rossini et al. 2011) and TGF- $\beta$  (Lorenzo et al. 2008; Rico et al. 2010) in RA. There is also evidence that others pathways, such as the Wnt signaling pathway and the IL-17 cytokine family, are critical in RA but were not described in our model. Owing to the model complexity, making such assumptions is essential to describe our experimental data together.

To fully appreciate the interplay between these cytokines, biomarkers, and the bone turnover process, disease progression and dynamic profiles of all involved mediators under the condition where only one single component is in effect or inhibited (for example, by the use of specific inhibitors such as TNF- $\alpha$ , IL-1, IL-6, or RANKL antagonists) would be necessary. This type of information is essential for better assessment of the interactions

between different mediators, in the same manner that PK/PD information for the individual drugs is required in drug–drug interaction studies. Incorporation of other signaling pathways is critical for better understanding of the entire mechanisms governing RA and bone destruction. Subsequent studies may be designed and help in resolving these relationships.

## Conclusions

A mechanism-based systems model is developed to describe the immune pathways involved in bone destruction during disease progression in CIA rats. The interplay between GR, proinflammatory cytokines (TNF- $\alpha$ , IL-1 $\beta$ , IL-6), RANK/RANKL/OPG system, and BMD is characterized. The disease progressions of RANKL, OPG, TRACP-5b, and BMD are shown to be controlled by the disease progressions of cytokines and endogenous CST. DEX suppresses the expressions of cytokines and RANKL after dosing and subsequently modulates the activities of bone-forming osteoblasts and bone-resorbing osteoclasts. Although the model only describes a simple version of probable bone remodeling processes and there are probably other crucial pathways that may require consideration, it allows the characterization of all measured biomarkers under CIA disease progression and the intervention of DEX. Future experiments may be conducted to study the crosstalk between the cytokines, the RANK/RANKL/OPG system, and other mediators such as the Wnt signaling family, PTH, and calcium and investigate how they function on the bone remodeling process in RA.

## Acknowledgements

This work was supported by funding from NIH Grant GM 24211 and a fellowship for Lon from Amgen, Inc. We thank Marina Stolina from Amgen, Inc. for sharing the protocol for paw homogenate preparation, and Yanlin Wang for her technical support in the animal experiments.

## Author Contributions

*Participated in research design:* Lon, DuBois, Earp, Almon, Jusko. *Conducted experiments:* Lon, DuBois, Earp. *Performed data analysis:* Lon, Earp. *Wrote or contributed to the writing of the manuscript:* Lon, DuBois, Earp, Almon, Jusko.

## Disclosure

None declared.

## References

- Af Ekenstam E, Benson L, Hallgren R, Wide L, Ljunghall S (1990). Impaired secretion of parathyroid hormone in patients with rheumatoid arthritis: relationship to inflammatory activity. *Clin Endocrinol* 32: 323–328.
- Alatalo SL, Ivaska KK, Waguespack SG, Econs MJ, Vaananen HK, Halleen JM (2004). Osteoclast-derived serum tartrate-resistant acid phosphatase 5b in Albers-Schonberg disease (type II autosomal dominant osteopetrosis). *Clin Chem* 50: 883–890.
- Auphan N, DiDonato JA, Rosette C, Helmberg A, Karin M (1995). Immunosuppression by glucocorticoids: inhibition of NF-kappa B activity through induction of I kappa B synthesis. *Science* 270: 286–290.
- Bailer AJ (1988). Testing for the equality of area under the curves when using destructive measurement techniques. *J Pharmacokinet Biopharm* 16: 303–309.
- Braun T, Zwerina J (2011). Positive regulators of osteoclastogenesis and bone resorption in rheumatoid arthritis. *Arthritis Res Ther* 13: 235.
- Choy EH, Panayi GS (2001). Cytokine pathways and joint inflammation in rheumatoid arthritis. *N Engl J Med* 344: 907–916.
- Cooper C, Coupland C, Mitchell M (1995). Rheumatoid arthritis, corticosteroid therapy and hip fracture. *Ann Rheum Dis* 54: 49–52.
- Corrado A, Neve A, Maruotti N, Cantatore FP (2013). Bone effects of biologic drugs in rheumatoid arthritis. *Clin Dev Immunol* 2013: 945945.
- D'Argenio DZ, Schumitzky A, Wang X (2009). ADAPT 5 user's guide: pharmacokinetic/pharmacodynamic systems analysis software. Biomedical Simulations Resource, Los Angeles.
- Earp JC, Dubois DC, Molano DS, Pyszczynski NA, Almon RR, Jusko WJ (2008a). Modeling corticosteroid effects in a rat model of rheumatoid arthritis II: Mechanistic pharmacodynamic model for dexamethasone effects in Lewis rats with collagen-induced arthritis. *J Pharmacol Exp Ther* 326: 546–554.
- Earp JC, Dubois DC, Molano DS, Pyszczynski NA, Keller CE, Almon RR, et al. (2008b). Modeling corticosteroid effects in a rat model of rheumatoid arthritis I: mechanistic disease progression model for the time course of collagen-induced arthritis in Lewis rats. *J Pharmacol Exp Ther* 326: 532–545.
- Earp JC, Pyszczynski NA, Molano DS, Jusko WJ (2008c). Pharmacokinetics of dexamethasone in a rat model of rheumatoid arthritis. *Biopharm Drug Dispos* 29: 366–372.
- Earp JC, Dubois DC, Almon RR, Jusko WJ (2009). Quantitative dynamic models of arthritis progression in the rat. *Pharm Res* 26: 196–203.

- Gilbert L, He X, Farmer P, Boden S, Kozlowski M, Rubin J, et al. (2000). Inhibition of osteoblast differentiation by tumor necrosis factor- $\alpha$ . *Endocrinology* 141: 3956–3964.
- Goldring SR (2002). Bone and joint destruction in rheumatoid arthritis: what is really happening? *J Rheumatol Suppl* 65: 44–48.
- Halleen JM, Alatalo SL, Suominen H, Cheng S, Janckila AJ, Vaananen HK (2000). Tartrate-resistant acid phosphatase 5b: a novel serum marker of bone resorption. *J Bone Miner Res* 15: 1337–1345.
- Hashizume M, Hayakawa N, Mihara M (2008). IL-6 trans-signalling directly induces RANKL on fibroblast-like synovial cells and is involved in RANKL induction by TNF- $\alpha$  and IL-17. *Rheumatology (Oxford)* 47: 1635–1640.
- Institute of Laboratory Animal Resources (1996). Guide for the Care and Use of Laboratory Animals, 7th ed.. Institute of Laboratory Animal Resources, Commission on Life Sciences, National Research Council, Washington DC.
- Jimi E, Nakamura I, Duong LT, Ikebe T, Takahashi N, Rodan GA, et al. (1999). Interleukin 1 induces multinucleation and bone-resorbing activity of osteoclasts in the absence of osteoblasts/stromal cells. *Exp Cell Res* 247: 84–93.
- Kanbe K, Nakamura A, Inoue Y, Hobo K (2012). Osteoprotegerin expression in bone marrow by treatment with tocilizumab in rheumatoid arthritis. *Rheumatol Int* 32: 2669–2674.
- Karmakar S, Kay J, Gravalles EM (2010). Bone damage in rheumatoid arthritis: mechanistic insights and approaches to prevention. *Rheum Dis Clin North Am* 36: 385–404.
- Kim HJ, Zhao H, Kitaura H, Bhattacharyya S, Brewer JA, Muglia LJ, et al. (2006). Glucocorticoids suppress bone formation via the osteoclast. *J Clin Invest* 116: 2152–2160.
- Klareskog L, Catrina AI, Paget S (2009). Rheumatoid arthritis. *Lancet* 373: 659–672.
- Kobayashi K, Takahashi N, Jimi E, Udagawa N, Takami M, Kotake S, et al. (2000). Tumor necrosis factor  $\alpha$  stimulates osteoclast differentiation by a mechanism independent of the ODF/RANKL-RANK interaction. *J Exp Med* 191: 275–286.
- Kudo O, Sabokbar A, Pocock A, Itonaga I, Fujikawa Y, Athanasou NA (2003). Interleukin-6 and interleukin-11 support human osteoclast formation by a RANKL-independent mechanism. *Bone* 32: 1–7.
- Lam J, Takeshita S, Barker JE, Kanagawa O, Ross FP, Teitelbaum SL (2000). TNF- $\alpha$  induces osteoclastogenesis by direct stimulation of macrophages exposed to permissive levels of RANK ligand. *J Clin Invest* 106: 1481–1488.
- Lemaire V, Tobin FL, Greller LD, Cho CR, Suva LJ (2004). Modeling the interactions between osteoblast and osteoclast activities in bone remodeling. *J Theor Biol* 229: 293–309.
- Liu XH, Kirschenbaum A, Yao S, Levine AC (2005). Cross-talk between the interleukin-6 and prostaglandin E(2) signaling systems results in enhancement of osteoclastogenesis through effects on the osteoprotegerin/receptor activator of nuclear factor- $\kappa$ B (RANK) ligand/RANK system. *Endocrinology* 146: 1991–1998.
- Liu D, Lon HK, Dubois DC, Almon RR, Jusko WJ (2011). Population pharmacokinetic-pharmacodynamic-disease progression model for effects of anakinra in Lewis rats with collagen-induced arthritis. *J Pharmacokinet Pharmacodyn* 38: 769–786.
- Lon HK, Liu D, Zhang Q, DuBois DC, Almon RR, Jusko WJ (2011). Pharmacokinetic-pharmacodynamic disease progression model for effect of etanercept in Lewis rats with collagen-induced arthritis. *Pharm Res* 28: 1622–1630.
- Lorenzo J, Horowitz M, Choi Y (2008). Osteoimmunology: interactions of the bone and immune system. *Endocr Rev* 29: 403–440.
- Ma T, Miyanishi K, Suen A, Epstein NJ, Tomita T, Smith RL, et al. (2004). Human interleukin-1-induced murine osteoclastogenesis is dependent on RANKL, but independent of TNF- $\alpha$ . *Cytokine* 26: 138–144.
- Nanes MS (2003). Tumor necrosis factor- $\alpha$ : molecular and cellular mechanisms in skeletal pathology. *Gene* 321: 1–15.
- Nedelman JR, Gibiansky E, Lau DT (1995). Applying Bailer's method for AUC confidence intervals to sparse sampling. *Pharm Res* 12: 124–128.
- Nelson CA, Warren JT, Wang MW, Teitelbaum SL, Fremont DH (2012). RANKL employs distinct binding modes to engage RANK and the osteoprotegerin decoy receptor. *Structure* 20: 1971–1982.
- Palmqvist P, Persson E, Conaway HH, Lerner UH (2002). IL-6, leukemia inhibitory factor, and oncostatin M stimulate bone resorption and regulate the expression of receptor activator of NF- $\kappa$ B ligand, osteoprotegerin, and receptor activator of NF- $\kappa$ B in mouse calvariae. *J Immunol* 169: 3353–3362.
- Peterson MC, Riggs MM (2010). A physiologically based mathematical model of integrated calcium homeostasis and bone remodeling. *Bone* 46: 49–63.
- Peterson MC, Riggs MM (2012). Predicting nonlinear changes in bone mineral density over time using a multiscale systems pharmacology model. *CPT Pharmacometrics Syst Pharmacol* 1: e14.
- Pivonka P, Zimak J, Smith DW, Gardiner BS, Dunstan CR, Sims NA, et al. (2008). Model structure and control of bone remodeling: a theoretical study. *Bone* 43: 249–263.
- Pivonka P, Zimak J, Smith DW, Gardiner BS, Dunstan CR, Sims NA, et al. (2010). Theoretical investigation of the role of the RANK-RANKL-OPG system in bone remodeling. *J Theor Biol* 262: 306–316.

- Post TM, Schmidt S, Peletier LA, de Greef R, Kerbusch T, Danhof M (2013). Application of a mechanism-based disease systems model for osteoporosis to clinical data. *J Pharmacokinet Pharmacodyn* 40: 143–156.
- Rico MC, Rough JJ, Del Carpio-Cano FE, Kunapuli SP, DeLa Cadena RA (2010). The axis of thrombospondin-1, transforming growth factor beta and connective tissue growth factor: an emerging therapeutic target in rheumatoid arthritis. *Curr Vasc Pharmacol* 8: 338–343.
- Rioja I, Bush KA, Buckton JB, Dickson MC, Life PF (2004). Joint cytokine quantification in two rodent arthritis models: kinetics of expression, correlation of mRNA and protein levels and response to prednisolone treatment. *Clin Exp Immunol* 137: 65–73.
- Rissanen JP, Suominen MI, Peng Z, Halleen JM (2008). Secreted tartrate-resistant acid phosphatase 5b is a Marker of osteoclast number in human osteoclast cultures and the rat ovariectomy model. *Calcif Tissue Int* 82: 108–115.
- Rossini M, Bagnato G, Frediani B, Iagnocco A, La Montagna G, Minisola G, et al. (2011). Relationship of focal erosions, bone mineral density, and parathyroid hormone in rheumatoid arthritis. *J Rheumatol* 38: 997–1002.
- Schmidt S, Post TM, Peletier LA, Boroujerdi MA, Danhof M (2011). Coping with time scales in disease systems analysis: application to bone remodeling. *J Pharmacokinet Pharmacodyn* 38: 873–900.
- Stolina M, Adamu S, Ominsky M, Dwyer D, Asuncion F, Geng Z, et al. (2005). RANKL is a marker and mediator of local and systemic bone loss in two rat models of inflammatory arthritis. *J Bone Miner Res* 20: 1756–1765.
- Stolina M, Bolon B, Dwyer D, Middleton S, Duryea D, Kostenuik PJ, et al. (2008). The evolving systemic and local biomarker milieu at different stages of disease progression in rat collagen-induced arthritis. *Biomarkers* 13:692–712.
- Stolina M, Bolon B, Middleton S, Dwyer D, Brown H, Duryea D, et al. (2009). The evolving systemic and local biomarker milieu at different stages of disease progression in rat adjuvant-induced arthritis. *J Clin Immunol* 29: 158–174.
- Suzuki M, Hashizume M, Yoshida H, Shiina M, Mihara M (2011). Intercellular adhesion molecule-1 on synovial cells attenuated interleukin-6-induced inhibition of osteoclastogenesis induced by receptor activator for nuclear factor kappaB ligand. *Clin Exp Immunol* 163: 88–95.
- Tanaka Y, Nakayamada S, Okada Y (2005). Osteoblasts and osteoclasts in bone remodeling and inflammation. *Curr Drug Targets Inflamm Allergy* 4: 325–328.
- Walsh NC, Crotti TN, Goldring SR, Gravallesse EM (2005). Rheumatic diseases: the effects of inflammation on bone. *Immunol Rev* 208: 228–251.
- Wei S, Kitaura H, Zhou P, Ross FP, Teitelbaum SL (2005). IL-1 mediates TNF-induced osteoclastogenesis. *J Clin Invest* 115: 282–290.
- Weinstein RS, Chen JR, Powers CC, Stewart SA, Landes RD, Bellido T, et al. (2002). Promotion of osteoclast survival and antagonism of bisphosphonate-induced osteoclast apoptosis by glucocorticoids. *J Clin Invest* 109: 1041–1048.
- Xu J, Tan JW, Huang L, Gao XH, Laird R, Liu D, et al. (2000). Cloning, sequencing, and functional characterization of the rat homologue of receptor activator of NF-kappaB ligand. *J Bone Miner Res* 15: 2178–2186.
- Yao Z, Li P, Zhang Q, Schwarz EM, Keng P, Arbin A, et al. (2006). Tumor necrosis factor-alpha increases circulating osteoclast precursor numbers by promoting their proliferation and differentiation in the bone marrow through up-regulation of c-Fms expression. *J Biol Chem* 281: 11846–11855.
- Zwerina J, Redlich K, Polzer K, Joosten L, Kronke G, Distler J, et al. (2007). TNF-induced structural joint damage is mediated by IL-1. *Proc Natl Acad Sci USA* 104: 11742–11747.

## Supporting Information

Additional Supporting Information may be found in the online version of this article:

**Data S1.** Derivations of equations 7-9.